

## Black Hole Masses of Intermediate-Redshift Quasars: Near Infrared Spectroscopy\*

Matthias Dietrich<sup>1</sup>, Smita Mathur<sup>1</sup>, Dirk Grupe<sup>2</sup>, Stefanie Komossa<sup>3</sup>,

dietrich@astronomy.ohio-state.edu

### ABSTRACT

We present near-infrared spectra of ten luminous, intermediate redshift quasars ( $z \simeq 2$ ;  $L_{bol} \simeq 10^{47}$  erg s<sup>-1</sup>), observed with SofI at the NTT of ESO/La Silla. With these rest-frame optical spectra we probe the  $H\beta - [O III]$  emission line region. Using the standard scaling relation involving the width of the  $H\beta$  line and the continuum luminosity, we measure black hole masses in the range of  $\sim 2 \times 10^9 \lesssim M_{bh} \lesssim 10^{10} M_{\odot}$  for these sources. We also used SDSS spectra to probe Mg II  $\lambda 2798$  and C IV  $\lambda 1549$  emission lines and used these for black hole mass measurements as well. The black hole mass estimates using C IV  $\lambda 1549$  are on average smaller by about 60% than those based on  $H\beta$ . The massive black holes we observe could not have grown by simple radiatively efficient accretion at the observed accretion rate starting from seeds of up to thousand solar masses. About 10% of the observed black hole mass must have been accumulated by earlier merger events and radiatively inefficient accretion. Radiatively efficient accretion would further grow these BHs to masses of several  $10^9 M_{\odot}$  in 2–3 e-folding times i.e., in several  $10^8$  yrs. This scenario is consistent with recent models of BH growth. The  $H\beta$ -based Eddington luminosity ratios are in the range of  $\sim 0.2$  to  $0.7$ , with an average of  $\langle L_{bol}/L_{edd} \rangle = 0.39 \pm 0.05$ . The  $L_{bol}/L_{edd}$  ratio distribution follows a log-normal distribution which is consistent with prior studies of quasars with comparable luminosity. We also find that the gas metallicity of the broad-line region is super-solar with  $\sim 3 Z/Z_{\odot}$ , based on

---

<sup>1</sup>Department of Astronomy, The Ohio State University, 140 West 18th Av., Columbus, OH 43210, USA

<sup>2</sup>Department of Astronomy and Astrophysics, Pennsylvania State University, 525 Davey Lab, University Park, PA 16802, USA.

<sup>3</sup>MPI für extraterrestrische Physik, Giessenbachstr., D-85748 Garching, Germany

\* Based on observations collected at the European Southern Observatory, La Silla, Chile, 073.B-0033(A)

$\text{N III]}\lambda 1750/\text{O III]}\lambda 1663$  and  $\text{N V}\lambda 1240/\text{C IV}\lambda 1549$  emission line ratios. We find no correlation of the gas metallicity with the optical  $\text{Fe II}$  emission line strength in our small sample, contrary to a recent suggestion.

## 1. Introduction

One of the major discoveries in the last few years has been the understanding that the quasar era is a function of luminosity; the peak of quasar X-ray luminosity function shifts to lower luminosity at progressively lower redshifts (e.g., Fiore et al. 2003; Ueda et al. 2003; Hasinger et al. 2005). This is often referred to as the downsizing of AGN activity with cosmic epoch. This result has been interpreted in terms of “anti-hierarchical BH growth” (e.g., Merloni 2004; Shankar et al. 2008a, 2008b) in which massive black holes (BHs) grow rapidly at high redshift while the lower-mass BHs grow at progressively lower redshifts. In particular, as per models of Marconi et al. (2004), BHs with masses more than  $10^9 M_\odot$  have attained 50% of their mass by  $z=2$ . These results are based on aggregate properties of quasars, viz. the X-ray luminosity functions and the X-ray background. It is imperative to test these models with direct probes of measured BH masses, BH growth times, and accretion rates of intermediate and high redshift quasars.

Another impetus to the BH mass quest came from observations showing that the mass of the nuclear black hole is intimately related to the bulge properties of its host galaxy. This showed that the BH formation and evolution is an integral part of galaxy formation process. This new paradigm of “BH–galaxy co-evolution” boosted the efforts to measure BH masses over a wide range. However, beyond  $cz \sim 1000 \text{ km s}^{-1}$  the BH sphere of influence cannot be resolved even for most massive BHs, even with HST. Thus, traditional methods of finding super-massive BHs, viz. stellar dynamics and gas dynamics, fail beyond a distance of 100 Mpc even for  $10^9 M_\odot$  BHs (Ferrarese & Ford 2005); this is closer than the distance to 3C 273. Therefore, beyond  $\sim 100$  Mpc, the only viable way to probe BHs is through their AGN activity.

Reverberation mapping (Peterson 1993) provides a direct way to measure BH masses of AGNs, albeit with an uncertainty of about a factor of 3 owing to the unknown geometry of the broad emission line region (BLR). Reverberation mapping, however, is a hard, time consuming experiment; accurate BH masses are measured for only about 37 AGNs so far (Peterson et al. 2004). For luminous quasars, the time required becomes particularly long because of their smaller variability and the larger radii of BLRs. Hence, reverberation mapping campaigns for a sample of luminous quasars are hard. However, this problem is overcome by using scaling relations calibrated against reverberation mapping. Using the

width of the  $H\beta$  emission line and the BLR radius–luminosity relation, BH masses can be reliably estimated (Kaspi et al. 2000; McLure & Dunlop 2004; Bentz et al. 2006) modulo a scaling factor of the order of unity.

$H\beta$  based BH masses have been estimated for a large number of AGNs (e.g., Boroson 2005; Woo & Urry 2002). At intermediate and high redshifts, however,  $H\beta$  shifts out of the optical band, hence Mg II and C IV lines are used to estimate BH masses at high and intermediate redshifts, respectively (e.g., McLure & Dunlop 2004; Vestergaard 2004; Dietrich & Hamann 2004; Warner et al. 2004). Several interesting results have come out of the studies using these mass estimates; e.g. the distribution of accretion rates relative to Eddington ( $\dot{m} = \dot{M}/\dot{M}_{\text{Eddington}}$ ) was found to be roughly Gaussian with a narrow width, and a peak around one third (Kollmeier et al. 2006).

Several studies have shown, however, that C IV based BH masses are systematically overestimated compared to the  $H\beta$  based masses (e.g., Baskin & Laor 2005; Shemmer et al. 2004; Sulentic et al. 2007), perhaps as a result of neglecting the influence of radiation pressure on the line emitting gas (Marconi et al. 2008; but see Netzer 2008). While  $H\beta$  based BH masses are well calibrated against reverberation mapping results, the same is not the case for C IV and in particular for Mg II scalings. Will the results based on C IV or Mg II masses hold when more accurate  $H\beta$  masses are used? In order to investigate this question,  $H\beta$  masses of intermediate redshift quasars need to be obtained.

We initiated a program for this purpose to obtain rest-frame optical spectra of ten intermediate redshift, luminous quasars with near infrared spectroscopy (using NTT of ESO; §2). Half of our intermediate-redshift quasars are classified as broad absorption line quasars (BAL QSOs — Bechtold et al. 2002; Hewett & Foltz 2003; Korista et al. 1993; Weymann et al. 1991). Thus, in addition to measuring BH masses at intermediate redshift, we can also try to understand the BAL QSO phenomenon.

BAL QSOs are a class of quasars showing strong, broad, and blue-shifted absorptions troughs which are generally ascribed to absorption by fast outflowing material (e.g., Weymann et al. 1981; Reichard et al. 2003). About 15 to 20% of all quasars are BAL QSOs. Out of these, about  $\sim 15\%$  show even absorption by low ionization species like Mg II  $\lambda 2798$  (Voit, Weymann, & Korista 1993). BAL QSOs have been suggested to represent an early stage of the active phase of a super-massive black hole which is still embedded in cool gas and dust which is blown out (e.g., Boroson & Meyers 1992; Becker et al. 2000). On the other hand, BAL QSOs may be similar to normal quasars and Seyfert 1 galaxies, just viewed through the outflow (e.g., Yuan & Wills 2003).

Various authors have noted the similarity between BAL QSOs and Narrow-Line Seyfert 1

(NLS1) galaxies. The class of NLS1 galaxies was introduced by Osterbrock & Pogge (1985), motivated by strong optical Fe II-emission, unusual narrow broad Balmer emission lines ( $\text{FWHM}(\text{H}\beta) < 2000 \text{ km s}^{-1}$ ), and relatively weak  $[\text{O III}]\lambda 5007$  emission ( $[\text{O III}]\lambda 5007/\text{H}\beta < 3$ ). Later it was recognized that many NLS1s exhibit a steep soft X-ray spectra (e.g., Boller et al. 1996; Grupe et al. 1998; Laor et al. 1997; Puchnarewicz et al. 1992) and some of them show strong and rapid X-ray variations (e.g., Boller et al. 1993; Leighly 1999). There are several lines of evidence that NLS1s are driven by less massive black holes with high accretion rates, close to the Eddington limit (Pounds, Done, & Osborne 1995; see Komossa 2008 for a recent review on NLS1s).

Boroson (2002) suggested that although BAL QSOs and Narrow-Line Seyfert 1 galaxies (NLS1s) have different black hole masses they both show similar high Eddington accretion rates ( $\dot{m} = \dot{M}/\dot{M}_{\text{edd}}$ ) which would support the idea that both groups are similar (Brandt & Gallagher 2000; Lawrence et al. 1997; Leighly et al. 1997), maybe AGNs in early evolutionary states as suggested by Grupe et al. (1999) and Mathur (2000a, b). Grupe et al. (2008) and Leighly et al. (2009) have recently reported on observations for the NLS1 galaxy WPVS 007 which were obtained over almost two decades in the X-ray (ROSAT, Chandra, Swift) and in the optical–ultraviolet domain. While its optical spectrum is that of a typical NLS1 galaxy, its UV spectrum shows BAL features which correspond to strong X-ray absorption.

We also studied correlations of the relative strength of the optical Fe II emission with properties of the broad-line region. Recently, Netzer & Traktenbrot (2007) have suggested that the  $\text{Fe II}_{\text{opt}}/\text{H}\beta$  ratio can be used as a metallicity indicator. Generally, the chemical composition of the BLR gas can be estimated using broad emission line ratios in the ultraviolet spectral range (for a review, see Hamann & Ferland 1999; Hamann et al. 2002). The key assumption is that secondary nitrogen production, i.e., the synthesis of nitrogen from existing carbon and oxygen via CNO burning in high mass stars (e.g., Tinsley 1979; Henry et al. 2000), is the dominant source for nitrogen, this results in  $N/O \propto O/H$  and hence  $N/H \propto (O/H)^2 \propto Z^2$ . This scaling of  $N/H$  with metallicity has been found for many H II-regions when the metallicity is above  $\sim 1/3$  to  $\sim 1/2$  solar (e.g., van Zee et al. 1998; Izotov & Thuan 1999; Henry et al. 2000; Pettini et al. 2002). For most of our targets we have spectra of the rest-frame ultraviolet wavelength range as well, so we investigate whether our targets show typical super-solar metallicity as has been observed for luminous quasars at high redshifts (e.g., Dietrich et al. 2003; Nagao et al. 2006). We also test the trend of  $\text{Fe II}_{\text{opt}}/\text{H}\beta$  with gas metallicity for our sample.

Throughout the paper spectral indexes are denoted as energy spectral indices with  $F_\nu \propto \nu^\alpha$ . Luminosities are calculated assuming a  $\Lambda$ CDM cosmology with  $\Omega_{\text{M}} = 0.3$ ,  $\Omega_{\Lambda} = 0.7$  and a Hubble constant of  $H_o = 70 \text{ km s}^{-1} \text{ Mpc}^{-1}$  (Spergel et al. 2003, 2007). All errors are

1- $\sigma$  unless stated otherwise.

## 2. Observation and Reduction

### 2.1. Observations

We have observed a sample of ten luminous quasars at intermediate redshifts of  $z \simeq 1.1$  to 2.2 (Tab. 1) to study the spectral properties of the  $H\beta - [O\text{ III}]$  line complex, the strength of the optical Fe II-emission, and to estimate the mass of the central super-massive black hole. The quasars were selected on the basis that (i) the  $H\beta - [O\text{ III}]$  emission line complex is redshifted to the J- or H-band, avoiding strong atmospheric absorption bands, (ii) rest-frame ultraviolet spectra exist, (iii) the quasars are accessible at the time of the observations and (iv) the quasars are sufficiently bright to record spectra with a cumulative signal-to-noise ratio of at least  $S/N \simeq 10$  in the continuum within reasonable integration times using a 4-m class telescope.

Five objects of our sample are Broad-Absorption Line quasars (BAL QSOs). To characterize BAL QSOs Weymann et al. (1991) suggested a BALnicity index, B.I., as a classifying property. The B.I. measures the strength of a displaced, blueshifted broad absorption feature which has to be separated from the line center by at least  $2000 \text{ km s}^{-1}$ . The BALnicity index can be considered as an equivalent width of the broad absorption trough in velocity space. The five BAL QSOs of our study show BALnicity indices in the range of  $B.I. \simeq 1000$  to  $\sim 2300 \text{ km s}^{-1}$  (Tab. 1). With five BAL QSOs and five non-BAL QSOs in our sample, we also study possible differences between the two classes.

We observed the quasars using the near-infrared imaging–spectrograph SofI at the 3.5 m NTT at La Silla/ESO from September 9 until 11, 2004 under photometric conditions. Based on the spatial profiles of the quasar spectra we estimated a seeing of  $\sim 1''$  and better during the observations, except for the beginning of the third night ( $\lesssim 2''$ ). In order to measure the  $H\beta - [O\text{ III}]$  line complex we used the blue grism to cover the near-infrared wavelength range  $\lambda \simeq 0.95$  to  $1.65 \mu\text{m}$ . A Hawai'i  $1024 \times 1024$  array from Rockwell was used in long-slit mode ( $1'' \times 280''$ ,  $0''.273/\text{pixel}$ ). The location of an object (quasar, standard star) was alternated along the slit for subsequent exposures to optimize sky correction. The individual integration time was set to 180 sec which result in total integration times ranging from 60 min up to 120 min (Tab. 1). For flux calibration and correction of the strong atmospheric absorption band that separate the J and H band wavelength range, several standard stars were observed during each night.

## 2.2. Reduction

The 2D near-infrared spectra of the quasars and standard stars were processed using standard MIDAS<sup>1</sup> software. The quasar and stellar spectra were corrected for dark current using dark frames with the same exposure time as the target spectra to account for exposure time dependent dark structures. Flat-field frames were taken in both lamp-on and lamp-off modes for each night. We subtracted the night sky intensity for each spectrum individually. The night sky fits were based on two regions,  $\sim 90''$  and  $\sim 150''$  wide on average and separated by  $\sim 11''$  relative to the spectrum of the quasar and the standard star, respectively. A  $3^{rd}$  order polynomial fit was used for each wavelength element to describe the spatial intensity distribution of the night sky emission. Xenon comparison spectra were recorded for wavelength calibration, which was based on  $\sim 20$  individual lines. The resulting wavelength range is  $\lambda \simeq 9385$  to  $16480 \text{ \AA}$ , with a step size of  $(6.9 \pm 0.7) \text{ \AA}/\text{pixel}$ . The spectral resolution, measuring the full width at half maximum (FWHM) of strong night sky emission lines and isolated lines in the xenon spectra, amounts to  $R \simeq 540$ .

We observed 19 standard stars with spectral type G0V to G3V during the three nights to correct for strong atmospheric absorption bands and to derive a sensitivity function. To describe the spectral energy distribution of the standard stars in the near-infrared wavelength range we computed black body spectra with effective temperatures typical for G0V to G3V stars (Pickles 1998). These black body spectra were scaled to match the apparent magnitudes of the observed standard stars using the relations given in Allen (2000) and Wamsteker (1981). In addition, we retrieved observed and calculated stellar spectra of corresponding spectral types (G0V to G3V), which are electronically available (Pickles 1998). Both types of these spectra were compared with the black body spectra. The observed stellar spectra and the corresponding black body spectra are similar within  $\sim 5\%$ , while the calculated spectra and the black body spectra differ by  $\sim 15\%$ . For consistency, we calculated sensitivity functions using scaled black body spectra. These are identical to the sensitivity functions based on individual standard stars within  $\sim 3\%$ . Hence, we calculated a mean sensitivity function which we used to calibrate the quasar spectra. To achieve an absolute flux scaling of the quasar spectra we used the 2 MASS broad band magnitudes (Cohen et al. 2003). The scaling factors varied in the range of  $\sim 0.8$  to  $\sim 1.6$ , with an average of  $1.09 \pm 0.08$ .

To correct for cosmic-ray events we compared the individual 1D spectra of each source with each other. For each quasar a weighted mean spectrum was calculated. The individual weights of the quasar spectra were given by the signal-to-noise ratio in the continuum. The width of the analyzed continuum windows was on average  $770 \pm 90 \text{ \AA}$  and they were

---

<sup>1</sup>Munich Image Data Analysis System, trade-mark of the European Southern Observatory

centered on average at  $\lambda \simeq 11170 \pm 310 \text{ \AA}$ . The resulting mean quasar spectra were corrected for atmospheric absorption using appropriately scaled atmospheric transmission functions which were obtained from the observed standard star spectra. In Figure 1 we present the flux calibrated near-infrared spectra of the intermediate-redshift quasars of this study.

### 3. Spectral Analysis

The near-infrared quasar spectra, covering the rest-frame optical spectral range, are displayed in Fig. 1. In addition, we also studied the observed optical spectra of our sample. These data were either taken from a sample of  $\sim 700$  quasars from Dietrich et al. (2002a) or from publicly available archival spectra of the Sloan Digital Sky Survey (SDSS; Adelman-McCarthy et al. 2006). These spectra cover the rest-frame ultraviolet range from Ly $\alpha$  to Mg II  $\lambda 2798$ , including the C IV  $\lambda 1549$  emission line.

#### 3.1. Reconstruction of the Quasar Spectra

Spectra of AGN contain contributions from several sources, including a power-law continuum, Balmer continuum emission, Fe II line emission in the optical and ultraviolet, emission from metal lines, and host galaxy emission. We used a multi-component fit approach to identify these components which is necessary to obtain reliable measurements of emission line properties (Wills et al. 1985; for more details see e.g., Dietrich et al. 2002b, 2005). We assume that the quasar spectra of this study can be described as a superposition of four components, (i) a power law continuum ( $F_\nu \sim \nu^\alpha$ ), (ii) a pseudo-continuum due to merging Fe II emission blends in the optical and (iii) ultraviolet, and (iv) Balmer continuum emission (Grandi 1982). For the rest-frame optical wavelength range it might be necessary to include the tail of the Paschen continuum emission also, as pointed out by Grandi (1982) and more recently by Korista & Goad (2001). However, the strength of the Paschen continuum emission is not well constrained. Hence, we do not add this component in our reconstruction model. In the case of luminous quasars, like the objects of this study, the contribution of the host galaxy is negligible. Therefore, no correction was applied for the host galaxy.

We used the rest frame optical Fe II template that has been extracted from observations of I Zw 1 by Boroson & Green (1992). This template covers the wavelength range  $\lambda\lambda 4250 \text{ \AA}$  to  $7000 \text{ \AA}$ . Recently, an alternative optical Fe II emission line template has been presented by Véron-Cetty et al. (2004) which in addition takes into account possible NLR contributions to the Fe II emission. Both templates are similar in general, but they differ in detail at

around  $\lambda \simeq 5000 \text{ \AA}$  and at  $\lambda \gtrsim 6400 \text{ \AA}$ . For the ultraviolet Fe II-emission we use the template provided by Vestergaard & Wilkes (2001) which is based on HST/FOS spectra of I Zw1.

The four components (power law continuum, Balmer continuum emission, optical and ultraviolet Fe II emission template), were simultaneously fitted to the continuum part of each quasar spectrum to determine the minimum  $\chi^2$  of the fit. The best fit of these components was subtracted before the emission line profiles of interest were further analyzed. To illustrate the method to separate the different components, we show the fit results for the spectrum of Q 2154–2005 in Figure 2. The residuum spectrum in the bottom panel of Figure 2 still exhibits relative strong residua in the wavelength ranges  $\lambda \simeq 3000 \text{ \AA}$  to  $\lambda \simeq 3500 \text{ \AA}$  and  $\lambda \simeq 3600 \text{ \AA}$  to  $\lambda \simeq 4200 \text{ \AA}$ . These residua can be ascribed to Fe II-emission which is not included in templates we use. Especially the strong feature at  $\lambda \simeq 3200 \text{ \AA}$  (UV multiplet M6 and M7) causes a strong residuum. The residuum blueward of the H $\gamma$  emission line might be caused by the broad Balmer emission lines of H $\delta$  and H $\epsilon$  which were not subtracted. The residuum at  $\lambda \simeq 5000 \text{ \AA}$  is similar to those found for SBS 1425+606 and PKS 2126–158 by Shemmer et al. (2004; their Figure 3). It might be partially due to very broad, redshifted H $\beta$  emission. Contributions from [O III] $\lambda\lambda$ 4959, 5007 emission appears to be unlikely.

### 3.2. Emission Line Profile Measurements

We used the residual quasar spectra which we obtained from the multi-component fit analysis (§ 3.1) to measure emission line properties such as width, strength, and flux. As we have demonstrated in Dietrich et al. (2003, 2005), the use of emission line profile templates allows us to separate the broad and narrow contributions to an observed profile; this facilitates determination of the integrated flux and the profile width, in particular for weak or blended emission lines.

To measure the properties of broad emission lines, we need to assess the contribution of the narrow component to the total profile, and correct for it. We used the [O III] $\lambda\lambda$ 4959, 5007 emission lines as templates for the narrow line profiles. The observed H $\beta$  line profile was reconstructed using a single broad or a broad and a high broad Gaussian profile together with an appropriately scaled narrow line profile. In Fig. 3 we show the results of the decomposition of the H $\beta$  and [O III] $\lambda\lambda$ 4959, 5007 emission lines, together with the power law continuum fit and the fitted optical Fe II emission template. For four of the observed quasars we could also analyze the H $\alpha$  region. The results of the continuum fit, the optical Fe II emission contribution, and the line profile fits for the H $\alpha$  region are displayed in Fig. 4. The H $\beta$  and also the H $\alpha$  profiles (Figs. 3 and 4) were corrected for narrow emission line contributions before measuring the profile width of the broad component. We also corrected the measured

observed profile width for the spectral resolution assuming that the spectral resolution of the spectrograph and the intrinsic profile width add in quadrature. In Table 2 we list these corrected profile widths of  $[\text{O III}]\lambda 5007$  and of the broad components of the  $\text{H}\alpha$ ,  $\text{H}\beta$ ,  $\text{Mg II}\lambda 2798$ , and  $\text{C IV}\lambda 1549$  emission lines.

For measuring the properties of emission lines in the ultraviolet, we fitted the  $\text{C IV}\lambda 1549$  line profile with a broad and narrow Gaussian component (e.g., Dietrich et al. 2003). The resulting fit to  $\text{C IV}$  emission profile was used as a template to measure the emission-line fluxes of  $\text{Ly}\alpha$ ,  $\text{N V}\lambda 1240$ ,  $\text{N IV}\lambda 1486$ ,  $\text{He II}\lambda 1640$ ,  $\text{O III}\lambda 1663$ ,  $\text{N III}\lambda 1750$ , if available. For these measurements the template profile width was allowed to vary and its location in velocity space was limited to a range of less than a few  $100 \text{ km s}^{-1}$  with respect to  $\text{C IV}\lambda 1549$ . In the case of Q 2212–1759 we used the profile of the  $\text{Si IV}\lambda 1402$  emission feature as a profile template. This way we could recover the strongly absorbed  $\text{C IV}\lambda 1549$  line profile. In addition, we were able to determine the line fluxes of  $\text{He II}\lambda 1640$ ,  $\text{O III}\lambda 1663$ , and  $\text{N III}\lambda 1750$ , employing an appropriately scaled  $\text{Si IV}\lambda 1402$  line profile. In Table 3 we present the line ratios of those emission lines which we used to estimate the gas chemical composition of the BLR gas of the quasars of this study (§4.2).

We estimated the uncertainties of the flux measurements from the fit using the scaled  $\text{C IV}\lambda 1549$  line profile template. For stronger lines like  $\text{Ly}\alpha 1216$ ,  $\text{N V}\lambda 1240$ , and  $\text{C IV}\lambda 1549$  the relative errors are of the order of  $\sim 10\%$  to  $15\%$ ; for the weaker lines, they are  $\sim 15\%$  to  $25\%$ . These errors do not take into account the continuum level uncertainties, which typically dominate in quasar spectral analysis. The uncertainty of the continuum level affects each line differently; the relative flux error is smaller for stronger lines like  $\text{C IV}\lambda 1549$ ,  $\sim 5\%$  to  $10\%$ , while for weaker lines like  $\text{N IV}\lambda 1486$  it may be as large as a factor of  $\sim 2$ .

## 4. Results

### 4.1. Super-Massive Black Hole Mass Estimates

Scaling relations are routinely used to estimate BH masses in AGNs (c.f., McGill et al. 2008). We applied the following scaling relations for black hole mass estimates of our luminous quasars.

$$m_{bh}(H\beta) = 8.13 \times 10^6 \left( \frac{\lambda L_{\lambda}(5100)}{10^{44} \text{ erg s}^{-1}} \right)^{0.50 \pm 0.06} \left( \frac{FWHM(H\beta 4861)}{1000 \text{ km s}^{-1}} \right)^2 M_{\odot} \quad (1)$$

$$m_{bh}(CIV\ 1549) = 4.57 \times 10^6 \left( \frac{\lambda L_{\lambda}(1350)}{10^{44} \text{erg s}^{-1}} \right)^{0.53 \pm 0.06} \left( \frac{FWHM(CIV\ 1549)}{1000 \text{ km s}^{-1}} \right)^2 M_{\odot} \quad (2)$$

$$m_{bh}(MgII\ 2798) = 3.20 \times 10^6 \left( \frac{\lambda L_{\lambda}(3000)}{10^{44} \text{erg s}^{-1}} \right)^{0.62 \pm 0.14} \left( \frac{FWHM(MgII\ 2798)}{1000 \text{ km s}^{-1}} \right)^2 M_{\odot} \quad (3)$$

Equations 1 and 2 are taken from Vestergaard & Peterson (2006) while equation 3 is from McLure & Dunlop (2004). To calculate the mass of the nuclear black hole using the relations above, we need to know the line widths and continuum luminosity. We used the FWHM of the emission line profile fits for the  $H\beta$ ,  $Mg\ II\ \lambda 2798$ , and  $CIV\ \lambda 1549$  emission lines, if available (Table 2) and the AGN continuum luminosity at  $\lambda = 5100\ \text{\AA}$ ,  $\lambda 3000\ \text{\AA}$ , and  $\lambda = 1350\ \text{\AA}$  (Tab. 4) which were derived from the power law component of the continuum fit. The resulting black hole masses for our sample quasars are given in Table 4. Vestergaard & Peterson (2006) estimate that the uncertainty in mass for a statistically large sample is about a factor of 3 to 4, but in cases of individual quasars the uncertainty can be a factor of 5 to 10.

The luminous intermediate redshift quasars of this study have black hole masses in the range of  $\sim 2 \times 10^9 M_{\odot} \lesssim M_{bh} \lesssim 10^{10} M_{\odot}$  using the  $H\beta$  emission line. We do not see any significant difference in the BH masses of BAL QSOs and non-BAL QSOs. The average BH mass of BAL QSOs is  $(4.6 \pm 1.4) \times 10^9 M_{\odot}$  while that of non-BAL QSOs is  $(5.1 \pm 1.2) \times 10^9 M_{\odot}$ . Given our small sample size, and the large inherent errors associated with BH mass measurements, this is perhaps not surprising.

For nine of the quasars these mass estimates can be compared with those based on the  $CIV\ \lambda 1549$  emission line. We find that the mass estimates based on  $H\beta$  tend to be on average higher than those using the  $CIV\ \lambda 1549$  emission line, by about  $\sim 60\%$  (Fig. 5a). The scatter of the average is quite large and it appears that the ratio of the mass estimates is either larger by a factor of  $\sim 2$  or smaller by a factor of  $\sim 0.4$ . However, within the uncertainties that are associated with radius-luminosity relations applied to single epoch spectra, these two mass estimates can be considered as consistent with each other. For seven of our ten luminous quasars we also compared the  $Mg\ II\ \lambda 2798$  based masses with those using  $H\beta$ . We find that the  $Mg\ II$  BH masses are a factor of  $\sim 3$  smaller than the  $H\beta$  based masses (Tab. 4, Fig. 5b). Although the difference of the estimated black hole masses has become smaller compared with earlier studies (e.g., Dietrich & Hamann 2004), the  $Mg\ II$ -based mass estimates are still smaller than those using  $H\beta$ .

We also applied the correlation between black hole mass and the velocity dispersion of its host galaxy bulge (the  $M_{bh}-\sigma_*$  relation, e.g. Tremaine et al. 2002) to estimate black hole masses. In particular, we use the relation given by Tremaine et al. (2002):

$$\log \frac{m_{bh}}{M_\odot} = (8.13 \pm 0.06) + (4.02 \pm 0.32) \log \frac{\sigma_*}{\sigma_o} \quad \text{with } \sigma_o = 200 \text{ km s}^{-1} \quad (4)$$

Because the spatial extent of the narrow emission line region (NLR) is of the order of several 100 pc, it has been suggested that the NLR gas dynamics is dominated by the bulge of the host galaxy (Whittle 1992). Hence, Nelson (2000) suggested that the FWHM([O III] $\lambda$ 5007) can be employed as a surrogate of the stellar velocity dispersion  $\sigma_*$ . In Figure 6 we plot the H $\beta$  based black hole masses against the [O III] $\lambda$ 5007 line width based masses of our luminous quasars. We find that the H $\beta$  based black hole masses are systematically larger. This is different from the trend seen at low redshift in NLS1 galaxies, which are either off-set from the M- $\sigma$  relation in the sense that H $\beta$ -based masses are smaller than [O III]-based masses (according to Mathur & Grupe 2005b), or, which do agree well with the M- $\sigma$  relation (according to Komossa & Xu (2007); after removing objects which had their entire [O III] profile dominated by outflow). Thus, it appears that at high redshift bulge growth lags behind that of the BH while at low redshift, some BHs are still growing in well-formed bulges. Alternatively, one may argue that the [O III] $\lambda$ 5007 emission line is not a good surrogate of bulge velocity dispersion  $\sigma_*$ .

Using the black hole mass estimates based on the broad H $\beta$  emission line (Tab. 4) and the optical continuum luminosity of the quasar continuum at  $\lambda = 5100 \text{ \AA}$  (Tab. 4), we computed the Eddington ratio  $L_{bol}/L_{edd}$ . The value of the conversion factor  $f_L$  between the monochromatic luminosity and the bolometric luminosity ( $L_{bol} = f_L \times \lambda L_\lambda(5100)$ ), is still debated in the literature (e.g., Elvis et al. 1994; Laor 2000; Netzer 2003; Richards et al. 2006). Recently, Marconi et al. (2004) suggested a luminosity dependent correction factor  $f_L$ . We assumed that the bolometric luminosity is given by  $L_{bol} = 9.74 \times \lambda L_\lambda(5100 \text{ \AA})$  and  $L_{bol} = 4.62 \times \lambda L_\lambda(1350 \text{ \AA})$ , respectively (Vestergaard 2004). To calculate the Eddington luminosity  $L_{edd}$ , we assumed that the gas is a mixture of hydrogen and helium ( $\mu = 1.15$ ), i.e.,  $L_{edd} = 1.45 \times 10^{38} M_{bh} / M_\odot \text{ erg s}^{-1}$ . We computed Eddington ratios using the C IV $\lambda$ 1549 and Mg II $\lambda$ 2798 line based black hole masses as well. The derived Eddington ratios are listed in Table 5. On average the quasars show  $\langle L_{bol}/L_{edd} \rangle = 0.39 \pm 0.05$ , ranging from 0.16 to 0.65 for black hole masses implied by the H $\beta$  emission line. The average Eddington ratio derived from the C IV $\lambda$ 1549 based black hole mass accounts to  $\langle L_{bol}/L_{edd} \rangle = 0.66 \pm 0.15$ , i.e. the scatter is higher with Eddington ratios ranging from 0.1 to 1.5. Once again, we do not see any significant difference between BAL QSOs ( $\langle L_{bol}/L_{edd} \rangle = 0.38 \pm 0.08$ ) and

non-BAL QSOs ( $\langle L_{bol}/L_{edd} \rangle = 0.41 \pm 0.07$ ). In Figure 7 the Eddington ratios  $L_{bol}/L_{edd}$  derived from the line profiles of the  $H\beta$ ,  $Mg\text{ II}\lambda 2798$ , and  $C\text{ IV}\lambda 1549$  emission lines are shown as a function of black hole mass  $M_{bh}$ . It can be seen that there is a clear trend toward higher Eddington ratios for less massive black holes. This is consistent with results of studies which show that less massive black holes appear to accrete matter at a higher rate, e.g., SMBHs in NLS1 galaxies (e.g., Mathur 2000a; Mathur et al. 2001). The same trend was also found by Netzer & Trakhtenbrot (2007) who studied nearly 10 000 quasars with  $z < 0.75$  from the SDSS.

#### 4.2. Estimates of the Central Gas Metallicity

Hamann & Ferland (1992, 1993) and Ferland et al. (1996) showed that emission line ratios involving  $N\text{ V}\lambda 1240$  are valuable metallicity indicators due to the secondary nature of nitrogen. To estimate the gas metallicity for the observed quasars we used the relations presented by Hamann et al. (2002). These relations are based on a thorough investigation of the influence of the spectral shape of the photoionizing continuum flux, gas density, the ionization parameter, and gas metallicity on emission-line ratios. They quantified the metallicity and  $N/H \propto Z^2$  dependence of various line ratios, including several generally weak intercombination lines. They favor  $N\text{ III}]\lambda 1750/O\text{ III}]\lambda 1663$ ,  $N\text{ V}\lambda 1240/(O\text{ VI}\lambda 1034 + C\text{ IV}\lambda 1549)$ ,  $N\text{ V}\lambda 1240/C\text{ IV}\lambda 1549$ , and  $N\text{ V}\lambda 1240/O\text{ VI}\lambda 1034$  line ratios as the most robust indicators to measure the gas chemical composition. For the quasars of this study we could not measure the  $O\text{ VI}\lambda 1034$  emission line. This leave us with two line ratios  $N\text{ III}]\lambda 1750/O\text{ III}]\lambda 1663$  and  $N\text{ V}\lambda 1240/C\text{ IV}\lambda 1549$  as the most reliable gas metallicity indicators.

In Table 3 we list the measured emission line ratios for the intermediate redshift quasars of this study. For four of the quasars at least three line ratios could be measured. Using the relations presented by Hamann et al. (2002) we transformed the observed emission line ratios into gas metallicity estimates. While the  $N\text{ V}/C\text{ IV}$  and the  $N\text{ III}]/O\text{ III}]$  emission line ratios are consistently indicating super-solar metallicities on average of  $Z \simeq 3Z_{\odot}$ , with a range of  $Z \simeq 1.4Z_{\odot}$  to  $\sim 10Z_{\odot}$ , the ratio  $N\text{ V}/\text{He II}$  yields about at least two times larger metallicities for Q 0150–202 and Q 2230+0232. However, it is known that the  $N\text{ V}/\text{He II}$  line ratio is not as reliable as  $N\text{ III}]\lambda 1750/O\text{ III}]\lambda 1663$  because  $\text{He II}$  is more sensitive to the actual spectral shape of the ionizing continuum (Hamann et al. 2002). For one of the two quasars we could measure the strength of the  $N\text{ IV}]\lambda 1486$  emission line and sub-solar metallicity is indicated for Q 2209–1842. However, it has to be taken into account that the  $N\text{ IV}]\lambda 1486$  emission line is generally weak and difficult to measure.

With Q 2212–1759 we have a quasar in our sample which belongs to the rare class

of exceptionally strong N III]λ1750 emitter (e.g., Bentz, Hall, & Osmer 2004; Dhanda et al. 2007; Jiang, Fan, & Vestergaard 2008). The strength of the N III]λ1750 line emission is comparable to the strength which is observed in Q 0353–383, the first quasar discovered of this class (Osmer & Smith 1980). Based on the N III]λ1750 / O III]λ1663 emission line ratio we estimate a gas metallicity of  $Z \simeq 11 \pm 2 Z_{\odot}$  (Tab. 3). This result is in good agreement with predictions by Baldwin et al. (2003), who suggested even higher metallicity of  $\sim 15 Z_{\odot}$ .

In summary, super-solar metallicity is indicated for the line emitting gas of these intermediate redshift quasars ( $z \simeq 2$ ) with  $Z \simeq 3 Z_{\odot}$ , based on the most suitable emission line ratios, N III]λ1750/O III]λ1663 and N Vλ1240/C IVλ1549. This result is consistent with earlier studies (e.g., Dietrich et al. 2003; Fields et al. 2005a, 2005b, 2007; Nagao et al. 2006) and it provides more support for metal enriched gas close to the super-massive black hole in an AGN.

### 4.3. Black Hole Growth Times

The time span that is necessary to build-up a SMBH with  $M_{bh} \gtrsim 10^9 M_{\odot}$ , can be estimated assuming accretion dominated growth of a single seed black hole on an e-folding time (e.g., Haiman & Loeb 2001; Shankar et al. 2004). We use the following equation from Volonteri & Rees (2006) to estimate the time necessary to assemble black hole masses which we found for our sample:

$$M_{bh}(t_{obs}) = M_{bh}^{seed}(t_o) \exp\left(\eta \frac{(1 - \epsilon)}{\epsilon} \frac{\tau}{t_{edd}}\right) \quad (5)$$

where  $\tau = t_{obs} - t_o$  is the time elapsed since the initial time,  $t_o$ , to the observed time,  $t_{obs}$ ;  $M_{bh}^{seed}$  is the seed black hole mass;  $\eta = L_{bol}/L_{edd}$  is the Eddington ratio;  $\epsilon$  is the efficiency of converting mass to energy, and  $t_{edd}$  is the Eddington time scale, with  $t_{edd} = \sigma_T c / 4\pi G m_p = 3.92 \times 10^8$  yr (Rees 1984). The Eddington time  $t_{edd}$  describes the time necessary to radiate at the Eddington luminosity the entire rest mass of an object. Various possibilities exist for the values of seed BH mass. In hierarchical models of structure formation the first baryonic objects which collapsed had masses of the order of  $\sim 10^4 - 10^6 M_{\odot}$  (e.g., Silk & Rees 1998; Shibata & Shapiro 2002; Bromm & Loeb 2003); these can be considered as upper limits on the mass of the seed black hole  $M_{bh}^{seed}$ . In these models central massive objects form by effective angular momentum loss of the gas, either by turbulent viscosity or by global dynamical instabilities (Shlosman et al. 1989; Begelman et al. 2006). In a model suggested by Begelman et al. (2008) a massive seed black hole can also form in the center of such a structure and it grows by accreting the surrounding envelope. The black hole masses which

can be achieved within this scenario are in the range of  $10^4$  to  $10^6 M_\odot$ . Recent models of early star formation indicate that nearly metal free Pop III stars, formed at high-redshifts ( $z \gtrsim 20$ ), were predominantly very massive with  $M \gtrsim 100M_\odot$  (e.g., Fryer, Woosley, & Heger 2001; Abel, Bryan, & Norman 2002; Bromm, Coppi, & Larson 2002). Their stellar remnants are expected to be of the order of  $\sim 10M_\odot$  (e.g., Fryer 1999). However, some models for early star formation even indicate the possibility of black hole remnants with several times  $\sim 10^3M_\odot$  (Bond, Arnett, & Carr 1984; Devecchi & Volonteri 2008; Madau & Rees 2001).

We used equation (5) to derive the time  $\tau$  necessary to accumulate the  $H\beta$ -based black hole masses listed in Table 4, for seed black holes with masses of  $M_{bh}^{seed} = 10M_\odot$ ,  $10^3M_\odot$ , and  $10^5M_\odot$ , respectively. First, we assume that the black holes are accreting at the Eddington-limit, i.e.,  $\eta = L_{bol}/L_{edd} = 1.0$  and that the efficiency of converting mass into energy is  $\epsilon = 0.1$ . The resulting growth times are given in Table 6. Secondly, we computed the growth time using the observed Eddington ratios that are determined from  $H\beta$  based masses (Table 5). We find that the naive estimate of the time  $\tau$  to build-up a SMBH with masses as determined in this study is between several  $10^8$  yr and  $10^9$  yr in the case for Eddington limit accretors. However, if we use the observed Eddington ratios (Table 5) the growth time is almost always of the order of one to several Gyr. Although in almost all cases, except for Q 0019+0107, the estimated black hole mass can be assembled within the age of the universe at the observed redshift, the necessary time span is an order of magnitude longer than the duration of the quasar phase which is of the order of  $\sim 10^7$  to  $\sim 10^8$  yrs (e.g., Martini 2003a, 2003b; Martini & Weinberg 2001). Q 0019+0107 could build its black hole mass within the age of the universe at its redshift ( $z = 2.131$ ) only if the seed black hole was at least  $10^5 M_\odot$  and accreted matter for nearly 3 Gyr at the Eddington limit. This is highly unrealistic, taking into account estimates of quasar life times (e.g., Martini 2003a). However, this apparent problem can be easily resolved in the light of recent results of studies on the growth of super-massive black holes (e.g., Volonteri 2008; Volonteri et al. 2008). We will further discuss this in §5.3.

## 5. Discussion

### 5.1. Comparison with other Studies

#### 5.1.1. Black Hole Masses

As discussed in §4.1, we need to use the radius luminosity (R–L) relation to connect the  $H\beta$  emission line width to the mass of the nuclear black hole. There are several R–L relations published in literature, which differ in the slope  $\beta$  of the relation, with  $\beta$  ranging from 0.5 to 0.7 (e.g., Bentz et al. 2006; Kaspi et al. 2000, 2005; McGill et al. 2008; McLure &

Dunlop 2004; Vestergaard & Peterson 2006). In addition, Netzer et al. (2007) have suggested that the slope of the R–L relation might be luminosity dependent.

To study the impact of the slopes  $\beta$  of the R–L relation on black hole mass estimates, we calculated the black hole masses using a different slopes. First, we adopted the relation presented by Kaspi et al. (2000) who assumed  $\beta = 0.7$ . Using their relation we find that the black hole mass that are based on  $H\beta$  profile properties, would be overestimated by a factor of  $\sim 1.75 \pm 0.14$  independent of black hole mass, compared to the masses we derived (Tab. 4).

We also employed the relations that are presented in Kollmeier et al. (2006) who used the McLure & Jarvis (2002) relation with a slope  $\beta = 0.61$  for the  $H\beta$ -based R–L relation. For AGN at higher redshifts of their study the  $C\text{IV}\lambda 1549$  emission line was used (Vestergaard 2002;  $\beta = 0.7$ ). However, instead of using the relation given by McLure & Jarvis (2002) for  $\text{Mg}\text{II}\lambda 2798$  in the intermediate redshift range, Kollmeier et al. (2006) rescaled the  $\text{Mg}\text{II}$ -relation to be consistent with  $H\beta$ -based mass estimates. To achieve this goal they had to assume a steep slope of  $\beta = 0.88$  in the R–L relation for  $\text{Mg}\text{II}\lambda 2798$ . Their relations are designed to yield consistent black hole mass estimates for all AGNs, from local AGNs out to redshifts of  $z \simeq 5$ . We applied their relations for  $H\beta$ ,  $\text{Mg}\text{II}\lambda 2798$ , and  $C\text{IV}\lambda 1549$  to the high redshift quasars of this study. We find that their  $H\beta$ -based black hole mass estimates are about  $(1.1 \pm 0.1)$  times higher than our results. For the  $C\text{IV}\lambda 1549$ -based black holes mass estimates, they are in agreement with our analysis that the  $H\beta$ -based black hole masses are on average larger by about a factor of  $\sim 1.75$ . As far as the  $\text{Mg}\text{II}\lambda 2798$ -based masses are concerned, it is not surprising that their mass estimates are in good agreement with  $H\beta$  ( $\sim 1.1 \pm 0.3$ ). However, we find that the  $H\beta$ -based black hole masses are about  $3.1 \pm 0.8$  times larger than those derived from the  $\text{Mg}\text{II}\lambda 2798$  emission line.

Recent studies on the R–L relation indicate that the slope of the radius luminosity relation is close to  $\beta = 0.5$ , consistent with predictions of photoionization models (e.g., Davidson & Netzer 1979; Osterbrock & Ferland 2005). The presence of steeper slopes appear to be caused by not correcting for contributions of the host galaxy to the continuum luminosity (Bentz et al. 2006; Bentz et al. 2008).

While former studies indicated that the black hole masses that are based on the  $C\text{IV}\lambda 1549$  emission line profile width, are larger than those using the  $H\beta$  line, we found that the ratio of these mass estimates varies between  $\sim 0.15$  to  $\sim 2.7$ . For Q 2212–1759, the  $H\beta$ -based black hole mass is even  $\sim 5$  times larger. The former discrepancy might be caused by a steeper slope of  $\beta = 0.7$  (Vestergaard 2002), while revised and more recent studies imply a slope of  $\beta = 0.53 \pm 0.06$  for the R–L relation for  $C\text{IV}\lambda 1549$  (Vestergaard & Peterson 2006). The use of the  $C\text{IV}\lambda 1549$  emission line to estimate black hole masses is still under debate.

There are severe doubts about the reliability of this line (Baskin & Laor 2005; Netzer et al. 2007). It is generally assumed that  $H\beta$  and  $Mg\text{II}\lambda 2798$  which are low-ionization lines (LIL), arise in a disk-like structure and that the gas motion is gravitationally dominated. In contrast,  $C\text{IV}\lambda 1549$  is a high-ionization line (HIL) and its origin may be in a different part of the BLR (e.g., Elvis 2000; Murray & Chiang 1997,1998). As a HIL, it may have a stronger radial motion component. However, there are at least a few reverberation measurements for the  $C\text{IV}\lambda 1549$  emission line available (Collier et al. 2001; Clavel et al. 1991; Dietrich & Kollatschny 1995; Korista et al. 1995; O’Brien et al. 1998; Reichert et al. 1994; Wanders et al. 1997). Furthermore, it has been shown that the wings of the line vary simultaneously with the line core, within measurements uncertainties (Korista et al. 1995; O’Brien et al. 1998; Dietrich et al. 1998). This result excludes radial motions as dominant form of gas motion in the BLR. For several AGN the delay of LIL and HIL emission lines, like  $C\text{IV}\lambda 1549$ ,  $He\text{II}\lambda 4686$ ,  $He\text{II}\lambda 1640$ ,  $N\text{V}\lambda 1240$  could be studied. For all objects, with no exception it was found that the line response and the line profile width follow the expected relation for gravitationally bound gas motion, i.e. the radial motions can be neglected, playing only a minor role if at all (Peterson & Wandel 1999,2000; Onken & Peterson 2002; Kollatschny 2003). Nevertheless, as has been pointed out by Vestergaard (2004), objects which show strong  $C\text{IV}\lambda 1549$  line profile asymmetries, have to be handled with great care, and particularly for Narrow-Line Seyfert 1 galaxies the  $C\text{IV}\lambda 1549$  emission line is not suitable to estimate black hole masses. But in general, luminous quasars show well behaved profiles (for a more detailed discussion see Vestergaard 2004 and Vestergaard & Peterson 2006).

For the  $Mg\text{II}\lambda 2798$  emission line it should also be taken into account that the slope of the R–L relation is currently given as  $\beta = 0.62 \pm 0.14$  (McLure & Dunlop 2004), i.e., the uncertainty of the slope amounts to nearly  $\sim 25\%$ . These quite large uncertainty results into large uncertainties which we obtained for the black hole mass estimates that are based on the  $Mg\text{II}\lambda 2798$  emission line (Table 4). Thus, it has to be kept in mind when using a R–L relation based on other lines than the  $H\beta$  emission line to estimate black hole masses using single epoch spectra, that additional uncertainties affect the result (e.g., uncertainties in the slope of the R–L relation or additional radial outflow motion of the line emitting gas).

We studied whether the black hole mass can be estimated using the profile width of  $Mg\text{II}\lambda 2798$  and assuming that the slope of the R–L relation is  $\beta = 0.5$ , concurrent with the relations for  $H\beta$  and  $C\text{IV}\lambda 1549$  (Vestergaard & Peterson 2006). Thus, we used the black hole mass estimates based on the  $H\beta$  emission line profile and calculate the average scaling constant D, following

$$m_{bh}(H\beta) = m_{bh}(MgII) = D \left( \frac{\lambda L_{\lambda}(3000)}{10^{46} \text{erg s}^{-1}} \right)^{0.5} \left( \frac{FWHM(MgII\lambda 2798)}{1000 \text{ km s}^{-1}} \right)^2 M_{\odot} \quad (6)$$

For seven quasars in our sample we could analyze both the  $H\beta$ - and  $Mg\text{II}\lambda 2798$  line profile. Applying equation (6), we find an average  $D = (2.0 \pm 0.5) \times 10^8 M_{\odot}$ . Using this empirical constant  $D$ , we re-calculated the  $Mg\text{II}$ -based black hole masses; the results are given in Table 4, column (7). The black hole masses based on  $H\beta$  and on  $Mg\text{II}$  are in good agreement on average, by design, but in individual cases the estimates can differ by a factor of  $\sim 0.5$  to 1.6 (Tab. 4). This is consistent with the systematic uncertainty of black hole masses based on single epoch measurements (Vestergaard & Peterson 2006).

### 5.1.2. Eddington Luminosity Ratio Distributions

Although our sample size is small, consisting of ten intermediate-redshift luminous quasars, we compared the distribution of their Eddington luminosity ratio  $\eta = L_{bol}/L_{edd}$  with those of former, similar studies (e.g., Dietrich & Hamann 2004; Kollmeier et al. 2006; Netzer et al. 2007; Shemmer et al. 2004; Sulentic et al. 2004, 2006; Yuan & Wills 2003). We used the black hole mass estimates obtained from the  $H\beta$ ,  $Mg\text{II}$ , and  $C\text{IV}$  emission lines (Table 5) and the bolometric luminosity to derive the distribution of  $\eta$ . The Eddington ratios are binned in intervals of  $\Delta \log \eta = 0.25$  for better comparison with Kollmeier et al. (2006). In Figure 8 we show the  $L_{bol}/L_{edd}$  - distribution of our quasars in comparison with a sub-sample of AGES quasars (Kochanek et al. 2004; Kollmeier et al. 2006;  $N = 131$ ) and also with the quasar sample of Shemmer et al. (2004). The subsample of AGES quasars which has been investigated by Kollmeier et al. (2006), has redshifts of  $z > 1.2$  and bolometric luminosities in the range of  $10^{45} < L_{bol} < 10^{47} \text{ erg s}^{-1}$ . The quasar sample studied by Shemmer et al. (2004) and those of this study have similar redshifts of  $z \simeq 2.0$  and bolometric luminosities with  $L_{bol} > 10^{47} \text{ erg s}^{-1}$ .

The quasars of this study and of Shemmer et al. (2004) show a nearly identical distribution of the Eddington ratios (Fig. 8). A K-S test yields a probability of  $p = 1.0$  for both samples are being drawn from the same parent population. A K-S test applied to the  $\eta$  distributions of our quasar sample with the one found by Kollmeier et al. (2006) indicates that these quasars might be drawn from a different population ( $p = 0.036$ ). However, the shape of the cumulative distribution of the Eddington ratios of the AGES subsample is similar and it appears that our Eddington ratio distribution is slightly shifted to higher values (Fig. 8). The quasars of the Kollmeier et al. (2006) AGES sample are at least an order of magnitude less luminous than those of this study. Together with Shemmer et al. (2004) the current study extends the  $\eta$  - distribution to higher bolometric luminosities. In addition, we apply a different conversion factor ( $f_L = 9.74$  instead of  $f_L = 9$ ) to estimate the bolometric luminosity and we derive lower super-massive black hole masses. Thus, our estimates of

Eddington ratios are about  $\sim 20\%$  larger than those in Kollmeier et al. (2006).

Recently, Shemmer et al. (2004), Netzer & Trakhtenbrot (2007), and Netzer et al. (2007) studied a sample of 44 quasars in the redshift range of  $z \simeq 2$  to 3.4. These authors used a different transformation of the observed optical luminosity into a bolometric luminosity with  $L_{bol} = 7 \lambda L_{\lambda}(5100)$ . The factor  $f_L = 7$  (instead of our 9.74) is motivated by a study of Netzer (2003) which indicated a luminosity dependent transformation factor  $f_L$  in the range of 5 to 9 (see also Marconi et al. 2004). However, recently Richards et al. (2006) suggested that  $f_L = 10.3 \pm 2.0$  based on an analysis of SDSS quasar sample; use of  $f_L = 7$  would certainly underestimate the bolometric luminosity. In Netzer et al. (2007; their Fig. 9) the distribution of  $L_{bol}/L_{edd}$  appears to be narrow ( $\sim 1 dex$ ) but shifted to lower accretion rates compared to Kollmeier et al. (2006). We presume that some of the discrepancy arises from different values of  $f_L$  and different methods of measuring the black hole mass.

We also compared the Eddington ratio distribution with studies mentioned above. Netzer et al. (2007) studied high redshift quasars of lower bolometric luminosity ( $L_{bol} < 10^{47}$  erg s $^{-1}$ ) to search for luminosity effects in a joint re-analysis of the Shemmer et al. (2004) sample. The quasars of their sample were explicitly chosen to be 5 to 10 times less luminous than those of Shemmer et al. (2004). Quasars of comparable high luminosities, like those of this study, have been investigated by Yuan & Wills (2003), Sulentic et al. (2004, 2006), and Dietrich & Hamann (2004). In Figure 9 we display the individual  $L_{bol}/L_{edd}$  distributions and in addition the model fit for luminous high redshift quasars as found by Kollmeier et al. (2006). According to K-S tests the luminous intermediate-redshift quasars of this study are drawn from the same parent population like those of Shemmer et al. (2004), Dietrich & Hamann (2004), and Sulentic et al. (2004, 2006) since the null hypothesis has a probability of only  $p \simeq 4 \cdot 10^{-5}$ . The lower luminous quasar sample as studied by Kollmeier et al. (2006) and those of the Netzer et al. (2007) study might be drawn from a different parent population with a probability of  $p = 0.03$  to  $p = 0.05$ . The chance that the quasar samples of Kollmeier et al. (2006) and Netzer et al. (2007) are originated from different populations has a probability of about  $\sim 1.7 \cdot 10^{-5}$ , i.e. they might originate from the same parent population. However, for the Yuan & Wills (2003) sample we find that the intermediate-redshift quasars show an  $\eta$ -distribution which is shifted to higher Eddington ratios although the bolometric luminosity is in the same high luminosity range like those of Shemmer et al. (2004), Sulentic et al. (2004, 2006), and Dietrich & Hamann (2004).

The comparison of the Eddington ratio distributions indicate that there might be a dependence on the bolometric luminosity, i.e., at higher luminosities the mean Eddington ratio is shifted to higher values.

### 5.1.3. Correlations of $FWHM(H\beta)$ , $M_{bh}$ , $L_{bol}$ , and Eddington Ratio

The properties like black hole mass, Eddington ratio, and the range of  $Fe\ II_{opt}/H\beta$  ratios is consistent with the findings of an earlier study presented by Yuan & Wills (2003). Our luminous quasars occupy the same parameter space in  $L_{bol}$  vs.  $FWHM(H\beta)$ , indicating black masses in the range of  $10^9$  to  $10^{10} M_{\odot}$  which are accreting close to the Eddington limit.

In Figure 7 we present the distribution of the Eddington ratios as a function of the corresponding black hole mass for the luminous quasars of this study. There is a clear trend for lower Eddington ratios for more massive black holes. Correlations between  $L_{bol}/L_{edd}$  and  $M_{bh}$  have also come from X-ray studies; Piconcelli et al. (2005) have shown that the X-ray power-law slope ( $\Gamma$ ) anti-correlates with BH mass. (see also Boller et al. 1996; Brandt et al. 1995; Leighly et al. 1999; Grupe 2004; Shemmer et al. 2006). Since the X-ray power-law slope is an indicator of accretion rate relative to Eddington (Williams et al. 2004; Shemmer et al. 2006), the Piconcelli et al. observations imply an anti-correlation between the Eddington luminosity ratio and BH mass. This is similar to low-redshift results and suggests that the accretion rate relative to Eddington drops as the BHs grow (Grupe & Mathur 2004, Mathur & Grupe 2005a,b).

In Figures 10 and 11 we have plotted Eddington luminosity ratios as a function of the optical continuum luminosity  $\lambda L_{\lambda}(5100\text{\AA})$  and of black hole mass, respectively; only  $H\beta$ -based quantities are plotted. The filled diamonds represent our data, open diamonds are the data in Shemmer et al. (2004; their Table 2) and the open squares are from Netzer et al. (2007). Our data overlap with those of Shemmer et al. (2004). We find that both samples indicate an anti-correlation of the BH mass with the Eddington ratio (Figs. 7,11). This result is also consistent with that of Netzer & Trakhtenbrot (2007) for lower-redshift AGNs. Such an anti-correlation, however, is not surprising because both  $L_{bol}/L_{edd}$  and  $M_{bh}$  have been calculated using  $FWHM(H\beta)$  and  $L_{\lambda}(5100)$ . What is surprising is the result by Netzer et al. (2007) who, using a similar method, do not find such an anti-correlation. This is a direct result of the slope of the BLR radius–luminosity relation used by these authors. In their equation (1), the black hole mass depends upon  $L^{0.65}$ . As a result, the luminosity term remains in the  $L_{bol}/L_{edd}$  vs.  $M_{bh}$  relation. This is why, while the luminous quasars in their Figure 2 follow the anti-correlation between  $L_{bol}/L_{edd}$  and  $M_{bh}$ , the lower luminosity quasars are offset from the relation.

From the above discussion we may argue that our targets some of which are also BAL QSOs, are similar to NLS1s, in that they are accreting at high Eddington rates, different from the normal Seyfert 1 galaxies. On the other hand, as Figures 8 and 9 show, perhaps all high-z quasars are highly accreting (Grupe et al. 2004, 2006) and are high luminosity cousins of NLS1s, as being growing black holes (Mathur 2000a). At this stage, we do not

have sufficient data to test whether BAL QSOs occupy a different parameter space than other high- $z$  quasars.

### 5.2. Gas Metallicity and the $\text{Fe II}_{opt}/\text{H}\beta$ Ratio

The multi-component fit analysis of our quasar spectra provide the strength of the optical and ultraviolet  $\text{Fe II}$ -emission. Among the most prominent correlations of quasar properties is the increasing relative strength of the optical  $\text{Fe II}$ -emission with decreasing  $[\text{O III}]\lambda 5007$  strength. Recently, it has been suggested that the relative strength of the  $\text{Fe II}_{opt}$ -emission can be used as a metallicity indicator of the gas closely related to the central SMBH (Netzer & Trakhtenbrot 2007). This suggestion is based on the combination of two correlations; first, the correlation of the emission line ratio  $\text{N V}\lambda 1240/\text{C IV}\lambda 1549$  which can be used as a surrogate for gas metallicity, with the Eddington ratio (Shemmer et al. 2004) and second, the correlation of the  $\text{Fe II}_{opt}/\text{H}\beta$  ratio with the Eddington ratio (Netzer & Trakhtenbrot 2007).

In Figure 12 we display  $\text{N V}\lambda 1240/\text{C IV}\lambda 1549$  line ratio as well as the  $\text{Fe II}_{opt}/\text{H}\beta$  ratio as a function of the Eddington ratio,  $L/L_{edd}$ . The measured  $\text{N V}\lambda 1240/\text{C IV}\lambda 1549$  line ratio and the determined Eddington ratio place our luminous quasars in the range of super-solar quasars with high accretion rate, i.e. they follow the well founded correlation (Shemmer et al. 2004). We determined the gas metallicity for seven of our ten quasars at redshift  $z \simeq 2$  (Table 3). Thus, we could directly compare the strength of  $\text{Fe II}_{opt}/\text{H}\beta$  ratio with the estimated gas metallicity. In Figure 13 we display the  $\text{Fe II}_{opt}/\text{H}\beta$  ratio as a function of gas metallicity. To obtain a reliable estimate of the gas chemical composition, the determined metallicities are based on  $\text{N III}]\lambda 1750/\text{O III}]\lambda 1663$  and  $\text{N V}\lambda 1240/\text{C IV}\lambda 1549$ . These line ratios are suggested as the most suitable metallicity indicators (Hamann et al. 2002).

As can be seen in Figure 13, we do not detect a trend of the  $\text{Fe II}_{opt}/\text{H}\beta$  ratio with gas metallicity. However, this might be caused by the small number of studied quasars and the limited range in Eddington ratios. It is more than obvious that more measurements are needed.

### 5.3. Assembly of Super-Massive Black Holes

Based on a naive assumption that SMBH grow by accretion at the Eddington-Limit the black holes of the studied quasars can be built in about  $\sim 0.5$  Gyr if the seed black holes had masses of at least  $10^4 M_{\odot}$  (Table 6). This timescale, however, is larger than the estimated

life time for the active phase of quasars (Martini et al. 2003a, 2003b; see also Mathur et al. 2001). The situation becomes even more problematic when we note that the quasars do not accrete at the Eddington limit; the observed mean Eddington ratio is  $\sim 0.4$  (§4.1). Using this accretion rate and seed black holes as massive as  $M_{bh}(seed) \simeq 10^5 M_{\odot}$ , we find that for the ten quasars of this study the growth times are of the order of  $\sim 0.5$  Gyr to  $\sim 3$  Gyr. This strongly indicates that the growth of SMBHs is more complex than radiatively efficient mass-accretion. It has also been pointed out that radiatively efficient accretion tends to efficiently spin-up black holes (e.g., Cattaneo 2002; Volonteri et al. 2005, 2007, 2008). In these models the efficiency to convert matter into radiation can reach values of  $\epsilon \gtrsim 0.3$ . This makes growth timescales even longer; it would take about  $\sim 2$  Gyr to build-up black holes with  $\sim 10^9 M_{\odot}$ . Thus it seems that mergers and radiatively inefficient accretion must be important in early phases of the black hole growth (e.g., Marconi et al. 2004; Volonteri et al. 2007). In these models, the first  $\sim 10\%$  of the observed SMBH mass is accumulated via radiatively inefficient accretion (Volonteri 2008). Under the assumption that the radiatively efficient accretion started from seeds which already have  $10\%$  of the observed SMBH mass, it will take about  $\sim 10^8$  yr for quasars radiating at the Eddington-limit with  $\epsilon = 0.1$ . Using the observed Eddington ratios based on  $H\beta$  emission properties the growth times are in the range of  $\sim 1.5 \times 10^8$  yr to  $\sim 6.3 \times 10^8$  yr, with on average  $\sim 2.5 \times 10^8$  yr. This times agree quite well with the life times of the quasar phase (e.g., Martini 2003a, 2003b). If indeed the efficiency  $\epsilon$  is higher for close to Eddington accretors, e.g.  $\epsilon \simeq 0.25$  for  $L_{bol}/L_{edd} \simeq 1$ , then the implied growth times are about  $3 \times 10^8$  yr. For  $L_{bol}/L_{edd} \simeq 0.2$  and  $\epsilon \simeq 0.05$ , the growth time is about  $2 \times 10^8$  yr. Thus most of the mass of the SMBH can be accumulated during the active quasar phase, as suggested e.g. by Shankar et al. (2004) *only if a seed with 10% of the SMBH mass was already in place*. Perhaps this points toward an evolution of the Eddington ratio and a connection of the Eddington ratio and the efficiency of mass conversion  $\epsilon$  during the active phase. Initially, AGNs may accrete at close to the Eddington limit with high efficiency, like NLS1s appear to do. During this phase they also accrete most of their matter while later on the accretion rate decreases and the mass of the SMBH increases less (Mathur & Grupe 2005a,b).

## 6. Conclusions

Our goal was to measure  $H\beta$ -based BH masses of intermediate redshift quasars, for which the optical emission lines get redshifted into the infrared. We obtained near-infrared spectra of our sources using SofI with the NTT at ESO/La Silla. We find that the  $H\beta$  -based masses are not widely different from those based on C IV  $\lambda 1549$  line. The masses based on Mg II  $\lambda 2798$  are far more offset from the  $H\beta$  -based masses. Five of our sources are BAL QSOs and five

are non-BAL QSOs; we do not find any significant difference in their mass or Eddington luminosity ratio. A much larger sample would be needed to test any possible difference.

Even though our sample size is small, we find that the distribution of Eddington luminosity ratios follows a log-normal distribution which is consistent with former studies of luminous intermediate redshift quasars. Furthermore, we note a trend that for less luminous quasars the Eddington ratio distribution shifts to lower values.

X-ray observations have suggested that the Eddington luminosity ratio anti-correlates with black hole mass. Optical observations, using  $\text{FWHM}(\text{H}\beta)$  and  $L_\lambda(5100)$  for  $M_{bh}$ , result in a similar anti-correlation as long as the slope of the radius–luminosity relation is 0.5. The anti-correlation is smeared out if different values of the slope (for example 0.65) are used.

The gas metallicity of the broad-line region gas is estimated using the  $\text{N III]}/\text{O III]}$  and the  $\text{N V}/\text{C IV}$  emission line ratios. We find a metallicity of  $\sim 3 Z/Z_\odot$  which is consistent with previous results for intermediate redshift quasars. We compare these metallicities with the relative optical Fe II-emission for seven out of our ten quasars. We do not detect a trend between gas metallicity and  $\text{Fe II}_{opt}/\text{H}\beta$  in our small sample, contrary to a recent suggestion.

The measured BH masses of our sample are large,  $\sim 2 \times 10^9 \lesssim M_{bh} \lesssim 10^{10} M_\odot$ . Starting with seeds BHs up to about a thousand solar masses, these BHs could have grown by simple radiatively efficient accretion at the Eddington limit in less than about  $\sim 10^9$  yr. However, we do not observe these sources accreting at the Eddington limit. Using the observed accretion rate,  $< 0.39 \pm 0.05 >$ , the growth times become larger than the age of the Universe at the observed redshifts. SMBH growth must be more complex than simple radiatively efficient mass-accretion. At early stages of the black hole growth merger events and radiatively inefficient accretion must be important to build-up about the first  $\sim 10\%$  of the observed SMBH mass (Volonteri 2008). Under this assumption the observed SMBH mass can be reached within  $\sim 10^8$  yr for quasars radiating at the Eddington-limit with  $\epsilon = 0.1$ . Using the observed Eddington ratios based on  $\text{H}\beta$  emission properties the growth times are on average  $\sim 2.5 \times 10^8$  yr ( $\sim 1.5 \times 10^8$  yr to  $\sim 6.3 \times 10^8$  yr). These times are in the range estimated for the quasar phase.

MD acknowledges financial support from NSF grant AST-0604066 to the Ohio State University. SK thanks the ESO staff at La Silla for their help and hospitality.

## REFERENCES

- Abel, T., Bryan, G.L., & Norman, M.L. 2002, in 'Modes of Star Formation and the Origin of Field Population', ASP Conf. Series, Vol.285, p.213
- Adelman-McCarthy, J.K., et al. 2006, ApJS, 162, 38
- Allen, Astrophysical Quantities, 2000, ed. A.N. Cox, Springer
- Baldwin, J.A., Hamann, F., Korista, K.T., Ferland, G.J., Dietrich, M., & Warner, C. 2003, ApJ, 583, 649
- Baskin, A. & Laor, A. 2005, MNRAS, 356, 1029
- Bechtold, J., et al. 2002 ApJS, 140, 143
- Becker, R.H., et al. 2000, ApJ, 538, 72
- Begelman, M.C., Volonteri, M., & Rees, M.J. 2006, MNRAS, 370, 289
- Begelman, M.C., Rossi, E.M., & Armitage, P.J. 2008, MNRAS, 387, 1649
- Bentz, M.C., Hall, P.B., & Osmer, P.S. 2004, AJ, 128, 561
- Bentz, M.C., Peterson, B.M., Pogge, R.W., Vestergaard, M., & Onken, C.A. 2006, ApJ, 644, 133
- Bentz, M.C., Peterson, B.M., Netzer, H., Pogge, R.W., & Vestergaard, M. 2008, ApJ, in press, astro-ph/0812.2283v1
- Boller, T., Trümper, J., Molendi, S., et al. 1993, A&A, 279, 53
- Boller, T., Brandt, W.N., & Fink, H. 1996, A&A, 305, 53
- Bond, J.R., Arnett, W.D., & Carr, B.J. 1984, ApJ, 280, 825
- Boroson, T.A. 2002, ApJ, 565, 78
- Boroson, T.A. 2005, AJ, 130, 381
- Boroson, T.A. & Green, R.F. 1992, ApJS, 80, 109
- Boroson, T.A. & Meyers, K.A. 1992, ApJ, 397, 442
- Brandt, W.N., Pounds, K.A., & Fink, H. 1995, MNRAS, 273, L47

- Brandt, W.N. & Gallagher, S.C. 2000, *New.Astron.Rev.*, 44, 461
- Bromm, V., Coppi, P.S., & Larson, R.B. 2002, *ApJ*, 564, 23
- Bromm, V. & Loeb, A. 2003, *ApJ*, 596, 34
- Cattaneo A. 2002, *MNRAS*, 333, 353
- Clavel, J., et al. 1991, *ApJ*, 366, 64
- Cohen, M., Wheaton, Wm.A., & Megeath, S.T. 2003, *AJ*, 126, 1090
- Collier, S., et al. 2001, *ApJ*, 561, 146
- Davidson, K. & Netzer, H. 1979 *Rev Mod Phys.*, 51, 715
- Devecchi, B. & Volonteri, M. 2008, *ApJ*, submitted (astro-ph/0810.1057v1)
- Dhanda, N., Baldwin, J.A., Bentz, M.C., & Osmer, P.S. 2007, *ApJ*, 658, 804
- Dietrich, M. & Kollatschny, W. 1995, *A&A*, 303, 405
- Dietrich, M., et al. 1998, *apjs*, 115, 185
- Dietrich, M., et al. 2002b, *ApJ*, 564, 581
- Dietrich, M., et al. 2002a, *ApJ*, 581, 912
- Dietrich, M., et al. 2003, *ApJ*, 589, 722
- Dietrich, M. & Hamann, F. 2004, *ApJ*, 611, 761
- Dietrich, M., Crenshaw, D.M., & Kraemer, S.B. 2005, *ApJ*, 623, 700
- Elvis, M. 2000, *ApJ*, 545, 63
- Elvis, M., Wilkes, B.J., McDowell, J.C., Green, R.E., et al. 1994, *ApJS*, 95,1
- Ferland, G., et al. 1996, *ApJ*, 461, 683
- Ferrarese, L. & Ford, H. 2005, *Space Science Reviews*, 116, 523
- Fields, D.L., Mathur, S., Pogge, R.W., Nicastro, F., & Komossa, S. 2005a, *ApJ*, 620, 183
- Fields, D.L., Mathur, S., Pogge, R.W., Nicastro, F., Komossa, S., & Kronfold, Y. 2005b, *ApJ*, 634, 928

- Fields, D.L., Mathur, S., Krongold, Y., Williams, R., & Fabrizio, N. 2007, *ApJ*, 666, 828
- Fiore, F., et al. 2003, *A&A*, 409, 79
- Fryer, C.L. 1999, *ApJ*, 522, 413
- Fryer, C.L., Woosley, S.E., & Heger, A. 2001, *ApJ*, 550, 372
- Grandi, S.A. 1982, *ApJ*, 255, 25
- Grupe, D., Beuermann, K., Mannheim, K., & Thomas, H.-C. 1998, *A&A*, 330, 25
- Grupe, D., Beuermann, K., Mannheim, K., & Thomas, H.-C. 1999, *A&A*, 350, 805
- Grupe, D. 2004, *AJ*, 127, 1799
- Grupe, D., Mathur, S., Wilkes, B. & Elvis, M. 2004, *AJ*, 127, 1
- Grupe, D. & Mathur, S. 2004, *ApJ*, 606, L41
- Grupe, D., Leighly, K.M., & Komossa, S. 2008, *AJ*, 136, 2343
- Grupe, D., Mathur, S., Wilkes, B. & Osmer, P. 2006, *AJ*, 131, 55
- Haiman, Z. & Loeb, A. 2001, *ApJ*, 552, 459
- Hamann, F. & Ferland, G. 1992, *ApJ*, 391, L53
- Hamann, F. & Ferland, G. 1993, *ApJ*, 418, 11
- Hamann, F. & Ferland, G. 1999, *ARA&A*, 37, 487
- Hamann, F., Korista, K.T., Ferland, G.J., Warner, C., & Baldwin, J.A. 2002, *ApJ*, 564, 592
- Hasinger, G., Miyaji, T., & Schmidt, M. 2005, *A&A*, 441, 417
- Henry, R.B.C., Edmunds, M.G., & Köppen, J. 2000, *ApJ*, 541, 660
- Hewett, P.C. & Foltz, C.B. 2003, *AJ*, 125, 1784
- Izotov, Y.I. & Thuan, T.X. 1999, *ApJ*, 511, 639
- Jiang, L., Fan, X., & Vestergaard, M. 2008, *ApJ*, 679, 962
- Kaspi, S., et al. 2000, *ApJ*, 533, 631
- Kaspi, S., et al. 2005, *ApJ*, 629, 61

- Kelly, B.C., Bechtold, J., Trump, J.R., & Vestergaard, M. 2008, *ApJS*, 176, 353
- Kochanek, C., Eisenstein, D., Caldwell, N., Cool, R., Green, P., et al. 2004, *BAAS*, 205.9402K
- Kollatschny, W. 2003, *aap*, 407, 461
- Kollmeier, J.A., et al. 2006, *ApJ*, 648, 128
- Komossa, S. & Xu, D. 2007, *ApJ*, 667, L33
- Komossa, S. 2008, *RevMexAA*, 32, 86
- Korista, K.T., Voit, G.M., Morris, S.L., & Weymann, R.J. 1993, *ApJS*, 88, 357
- Korista, K.T., et al. 1995, *ApJS*, 97, 285
- Korista, K.T. & Goad, M.R. 2001, *ApJ*, 553, 695
- Laor, A. 2000, *ApJ*, 543, L111
- Laor, A., Fiore, F., Elvis, M., Wilkes, B.J., & McDowell, J. 1997, *ApJ*, 477, 93
- Lawrence, A., Elvis, M., Wilkes, B.J., McHardy, I., & Brandt, W.N. 1997, *MNRAS*, 285, 879
- Leighly, K.M. 1999, *ApJS*, 125, 297
- Leighly, K.M., Mushotzky, R.F., Nandra, K., & Forster, K. 1997, *ApJ*, 489, L25
- Leighly, K.M., Casebeer, D., Hamann, F., & Grupe, D. 2006, *HEAD 09.0737*, 38, 335
- Leighly, K.M., Grupe, D., et al. 2009, *ApJsubmitted*
- Madau, P. & Rees, M.J. 2001, *ApJ*, 551, L27
- Marconi, A., Risaliti, G., Gilli, R., Hunt, L.K., Maiolino, R., & Salvati, M. 2004, *MNRAS*, 351, 169
- Marconi, A., et al. 2008, *ApJ*, 678, 693
- Martini, P., Regan, M.W., Mulchaey, J.S., & Pogge, R.W. 2003a, *ApJ*, 589, 774
- Martini, P. & Schneider, D.P. 2003b, *ApJ*, 597, L109
- Martini, P. & Weinberg, D.H. 2001, *ApJ*, 547, 12
- Mathur, S. 2000a, *MNRAS*, 314, L17

- Mathur, S. 2000b, *New Astron. Rev.*, 44, 469
- Mathur, S. & Grupe, D. 2005a, *A&A*, 432, 463
- Mathur, S. & Grupe, D. 2005b, *ApJ*, 633, 688
- Mathur, S., Kuraszkiewicz, J., & Czerny, B. 2001, *NewA*, 6, 321
- McGill, K.L., Woo, T.-H., Treu, T., & Malkan, M.A. 2008, *ApJ*, 673, 703
- McLure, R.J. & Dunlop, J.S. 2004, *MNRAS*, 352, 1390
- McLure, R.J. & Jarvis, M.J. 2002, *MNRAS*, 337, 109
- Merloni, A. 2004, *MNRAS*, 353, 1035
- Murray, N. & Chiang, J. 1997, *ApJ*, 474, 91
- Murray, N. & Chiang, J. 1998, *ApJ*, 494, 125
- Nagao, T., Marconi, A., & Maiolino, R. 2006, *A&A*, 447, 157
- Nelson, C.H. 2000, *ApJ*, 544, L91
- Netzer, H. 2003, *ApJ*, 583, L5
- Netzer, H. 2008, astro-ph/0811.3251v2
- Netzer, H. & Trakhtenbrot, B. 2007, *ApJ*, 654, 754
- Netzer, H., Lira, P., Trakhtenbrot, B., Shemmer, O., & Cury, I. 2007, *ApJ*, 671, 1256
- O'Brien, P.T., et al. 1998, *ApJ*, 509, 163
- Onken, C.A. & Peterson, B.M. 2002, *ApJ*, 572, 746
- Osmer, P.S. & Smith, M.G. 1980, *ApJS*, 42, 333
- Osterbrock, D.E. & Ferland, G.J. 2005, *Astrophysics of Gaseous Nebulae and Active Galactic Nuclei*, 3<sup>rd</sup> edition, 2005, University Science Books
- Osterbrock, D.E. & Pogge, R.W. 1985, *ApJ*, 297, 166
- Peterson, B.M. 1993, *PASP*, 105, 274
- Peterson, B.M. & Wandel, A. 1999, *ApJ*, 521, L95

- Peterson, B.M. & Wandel, A. 2000, *ApJ*, 540, L13
- Peterson, B.M., et al. 2004, *ApJ*, 613, 682
- Pettini, M., Ellison, S.L., Bergeron, J., & Petitjean, P. 2002, *A&A*, 391, 21
- Pickles, A.J. 1998, *PASP*, 110, 863
- Piconcelli, E., Jimenez-Bailon, E., Guainazzi, M., Schartel, N., Rodriguez-Pascual, P.M., & Santos-Lleo, M. 2005, *A&A*, 432, 15
- Pounds, K.A., Done, C., & Osborne, J.P. 1995, *MNRAS*, 277, L5
- Puchnarewicz, E.M., et al. 1992, *MNRAS*, 256, 589
- Rees, M.J. 1984, *ARA&A*, 22, 471
- Reichard, T.A. 2003, *AJ*, 125, 1711
- Reichert, G.A., et al. 1994, *ApJ*, 425, 582
- Richards, G.T., et al. 2006, *ApJS*, 166, 740
- Shankar, F., Salucci, P., Granato, G.L., DeZotti G., & Danese, L. 2004, *MNRAS*, 354, 1020
- Shankar, F., Weinberg, D.H., & Miralda-Escudé, J. 2008a, *ApJin* press, astro-ph/0710.4488v1
- Shankar, F., Crocce, M., Miralda-Escudé, J., Fosalba, P., & Weinberg, D.H. 2008b, *ApJin* press, astro-ph/0810.4919v1
- Shemmer, O., et al. 2004, *ApJ*, 614, 547
- Shemmer, O., Brandt, W.N., Netzer, H., Maiolino, R., & Kaspi, S. 2006, *ApJ*, 646, L29
- Shibata, M. & Shapiro, S.L. 2002, *ApJ*, 572, L39
- Shlosman, I., Frank, J., & Begelman, M.C. 1989, *Nature*, 338, 45
- Silk, J. & Rees, M.J. 1998, *A&A*, 331, L1
- Spergel, D.N., et al. 2003, *ApJS*, 148, 175
- Spergel, D.N., et al. 2007, *ApJS*, 170, 377

- Sulentic, J.W., Stirpe, G.M., Marziani, P., Zananov, R., Calvani, M., & Braitto, V. 2004, *A&A*, 423, 121
- Sulentic, J.W., Repetto, P., Stirpe, G.M., Marziani, P., Dultzin-Hacyan, D., & Calvani, M. 2006, *A&A*, 456, 929
- Sulentic, J.W., Bachev, R., Marziani, P., Negrete, C.A., & Dultzin, D. 2007, *ApJ*, 666, 757
- Tinsley, B.M. 1979, *ApJ*, 229, 1046
- Tremaine, S., et al. 2002, *ApJ*, 574, 740
- Ueda, Y., Akiyama, M., Ohta, K., & Mitaji, T. 2003, *ApJ*, 598, 886
- van Zee, L., Salzer, J.J., & Haynes, M.P. 1998, *ApJ*, 497, L1
- Veron-Cetty, M.-P., Joly, M., & Veron, P. 2004, *A&A*, 417, 515
- Vestergaard, M. & Wilkes, B.J. 2001, *ApJS*, 134, 1
- Vestergaard, M. 2002, *ApJ*, 571, 733
- Vestergaard, M. 2004, *ApJ*, 601, 676
- Vestergaard, M. & Peterson, B.M. 2006, *ApJ*, 641, 689
- Viot, G.M., Weymann, R.J. & Korista, K.T. 1993, *ApJ*, 413, 95
- Volonteri, M. 2008, in *ESO Astrophysics Symposia 'Einstein's Relativistic and Astrophysics Legacy'*, Springer Verlag Berlin Heidelberg, p.174
- Volonteri, M., Lodato, G., & Natarajan, P. 2008, *MNRAS*, 383, 1079
- Volonteri, M., Sikora, M., & Lasota, J.-P. 2007, *ApJ*, 667, 704
- Volonteri, M., Madau, P., Quataert, E., & Rees, M.J. 2005, *ApJ*, 620, 69
- Volonteri, M. & Rees, M.J. 2006, *ApJ*, 650, 669
- Wamsteker, W. 1981, *A&A*, 97, 329
- Wanders, I., et al. 1997, *ApJS*, 113, 69
- Warner, C., Hamann, F., & Dietrich, M. 2004, *ApJ*, 608, 136
- Weymann, R.J., Carswell, R.F., & Smith, M.S. 1981, *ARA&A*, 19, 41

Weymann, R.J., Morris, S.L., Foltz, C.B., & Hewett, P.C. 1991, *ApJS*, 373, 23

Whittle, M. 1992, *ApJ*, 387, 121

Williams, R.J., Mathur, S., & Pogge, R.W. 2004, *ApJ*, 610, 737

Wills, B.J., Netzer, H., & Wills, D. 1985, *ApJ*, 288, 94

Woo, H.-J. & Urry, C.M. 2002, *ApJ*, 579, 530

Yuan, M.J. & Wills, B.J. 2003, *ApJ*, 593, L11

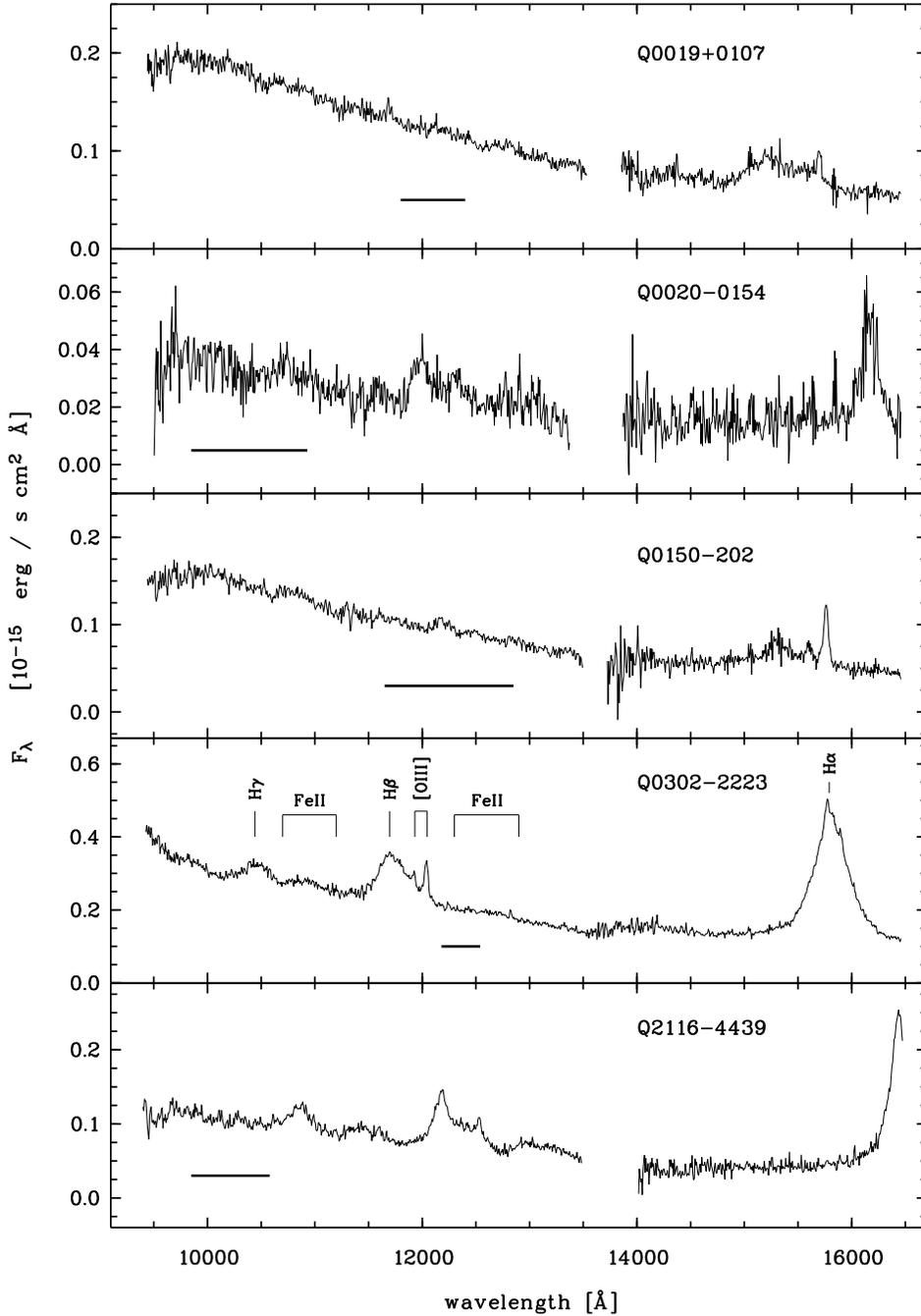


Figure 1 – The near-infrared spectra of the observed quasars. The flux density  $F_\lambda$  is given in units of  $10^{-15} \text{ erg s}^{-1} \text{ cm}^{-2} \text{ \AA}^{-1}$ . The horizontal bar at the bottom of each panel marks the range which is used to determine the weight of an individual spectrum.

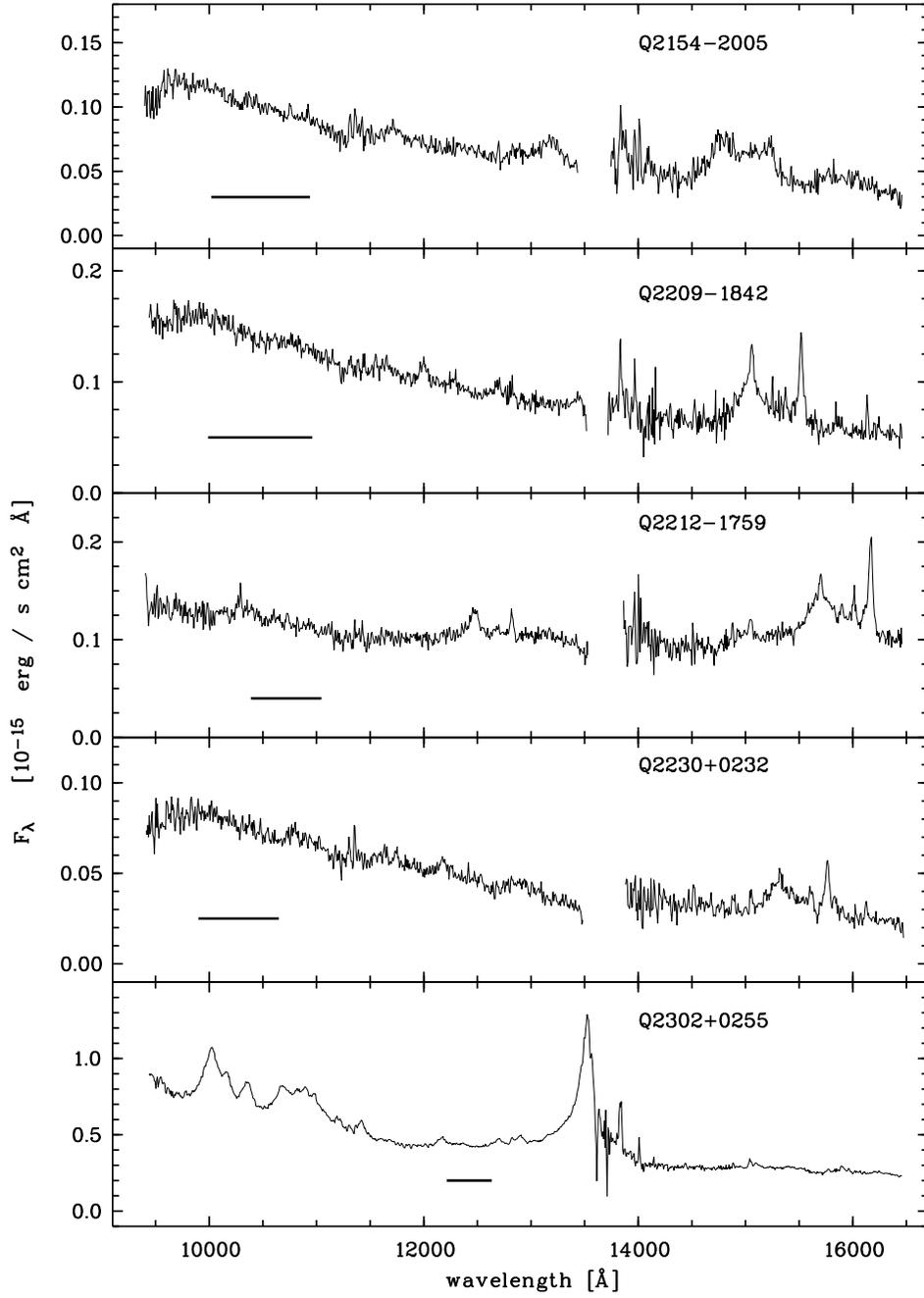


Figure 1 – continue

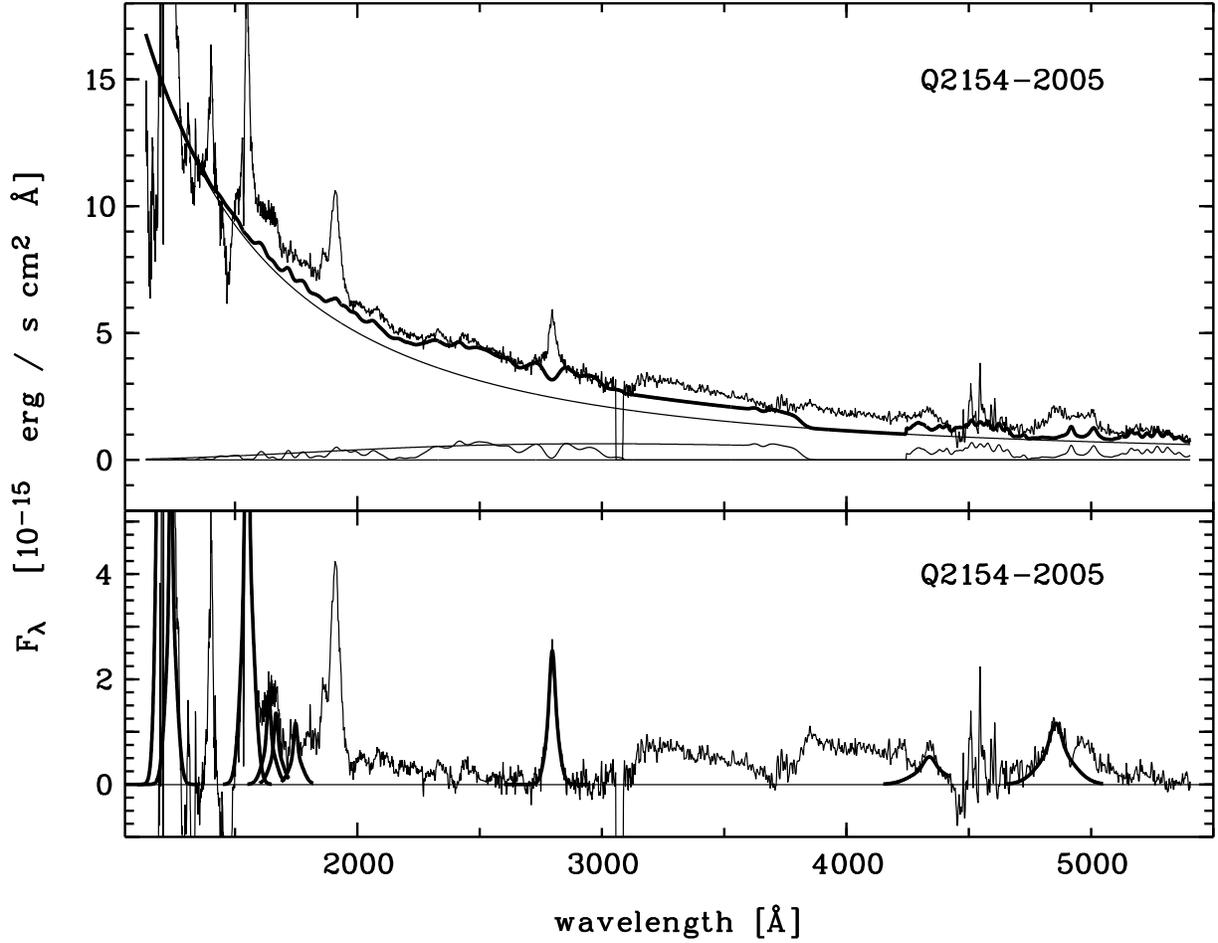


Figure 2 – Reconstruction of the UV-optical spectrum of Q 2154–2005 using a power law continuum, a Balmer continuum emission template, Fe II UV and Fe II optical emission templates. The fit is shown as the thick line. In the bottom panel the residual spectrum is shown. In addition, the broad emission line fits, used to determine the line strength and line profile width are displayed as thick lines.

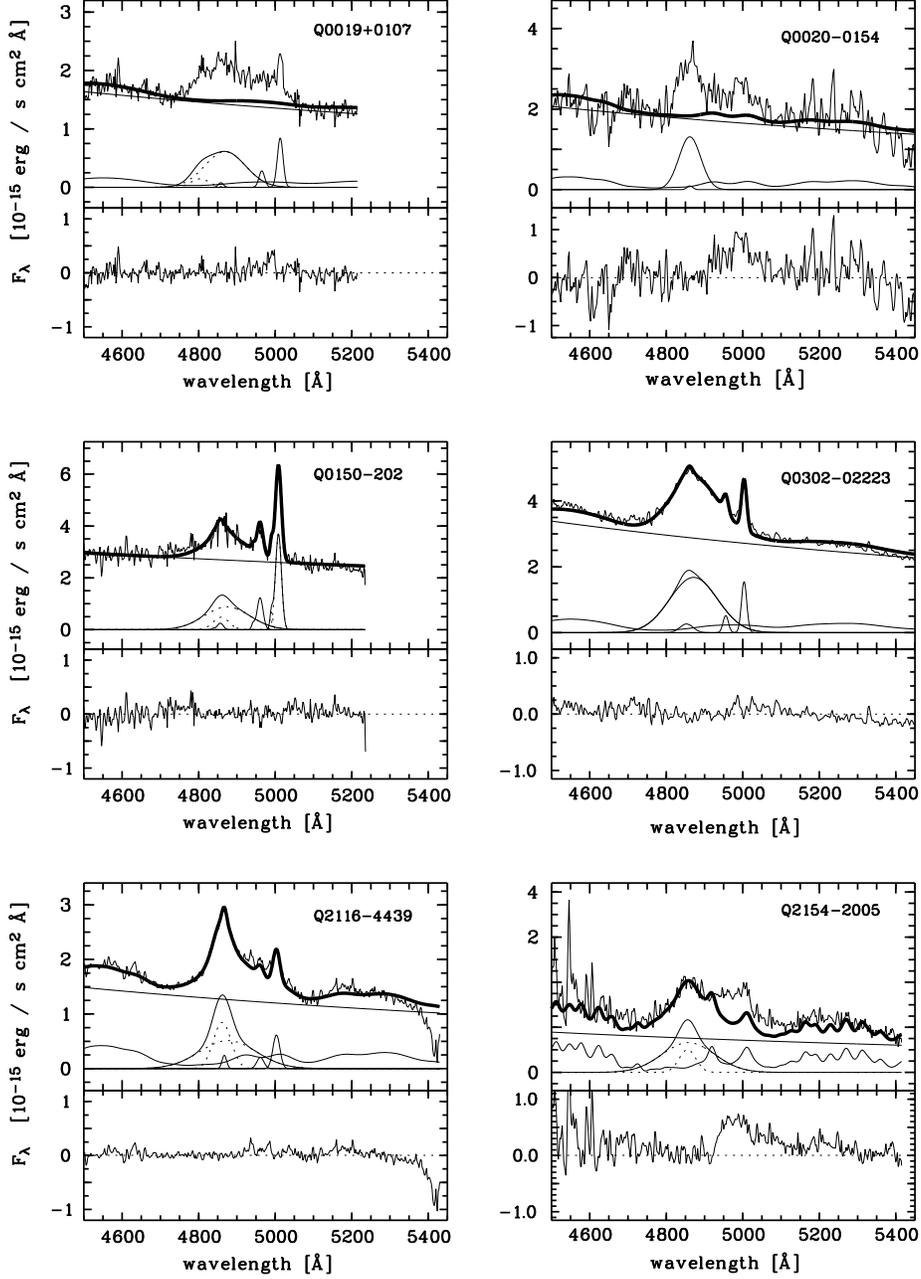


Figure 3 – Decomposition of the intermediate-redshift quasar spectra employing a multi-component fit. For each of the observed quasars the spectrum, transformed to the rest frame, is shown together with the power law continuum fit, an appropriately scaled Fe II optical emission template, the profile fits for H $\beta$  and [O III] $\lambda\lambda$ 4959, 5007 emission lines in the upper panel. The resulting fit is presented as thick solid line. In the lower panel the corresponding residual spectra are presented.

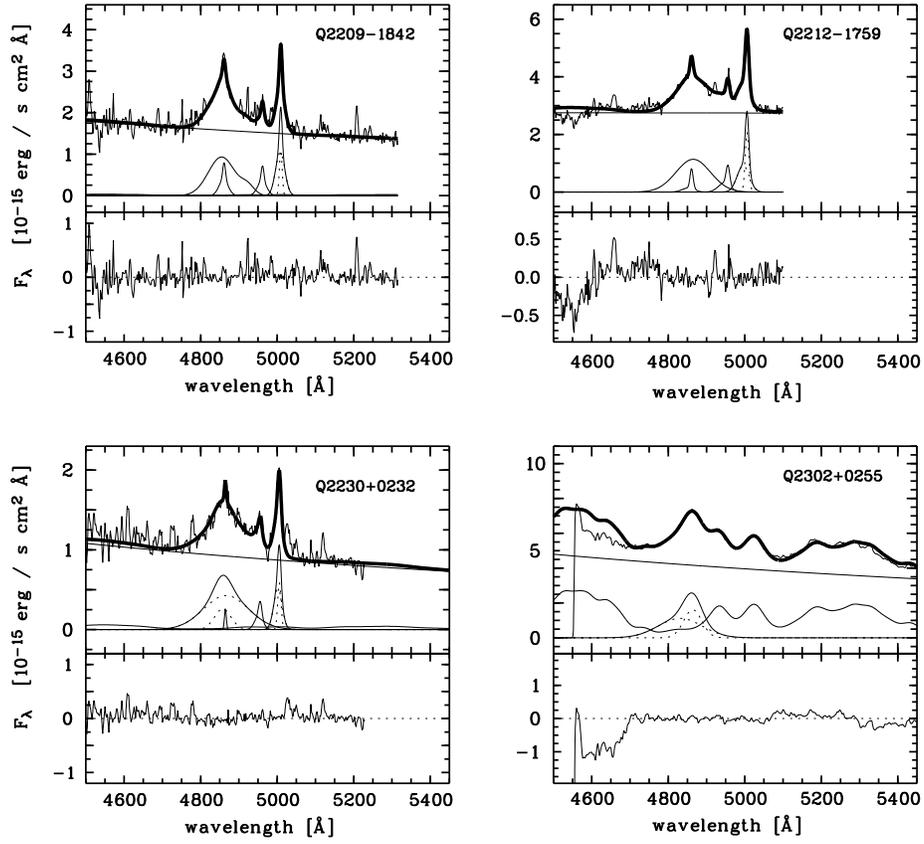


Figure 3 – continue

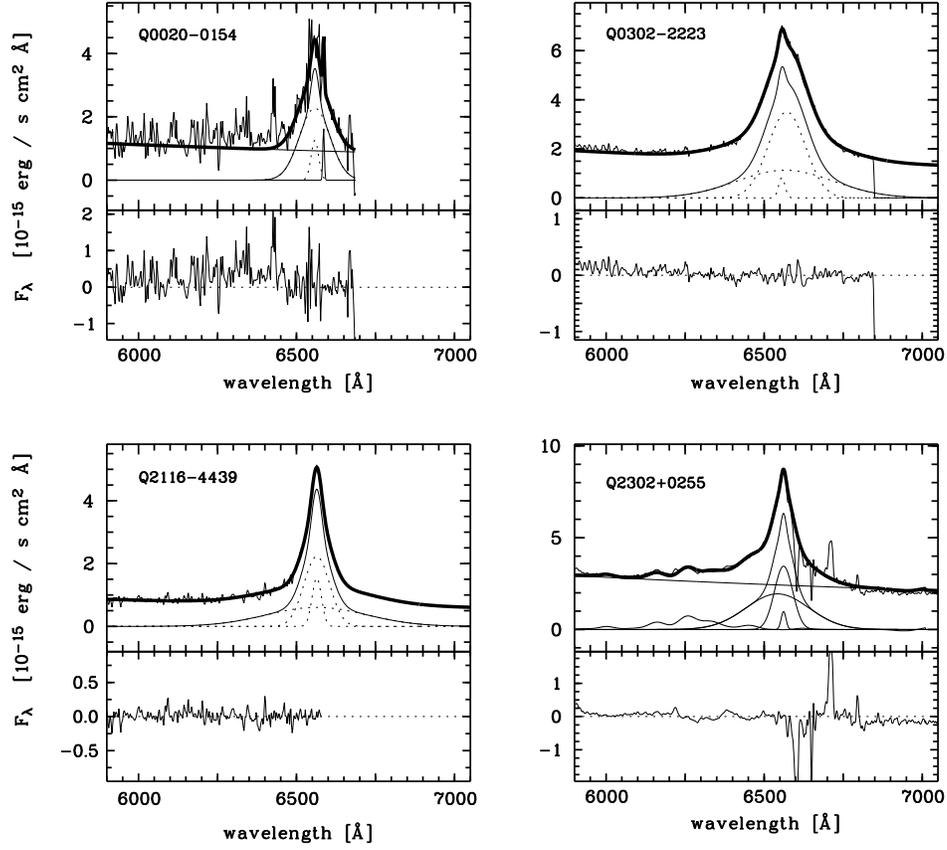


Figure 4 – Decomposition of the intermediate-redshift quasar spectra employing a multi-component fit for the H $\alpha$  emission line region.

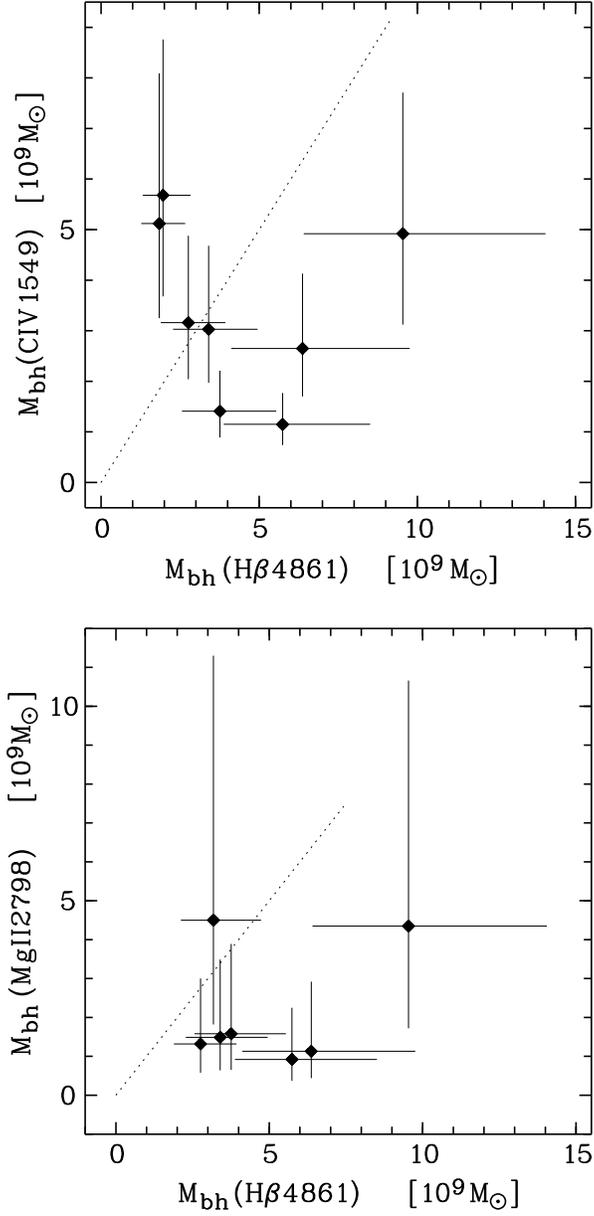


Figure 5 – Comparison of the black hole mass estimates based on the  $\text{H}\beta$  emission line profile and the optical continuum luminosity ( $\lambda = 5100 \text{ \AA}$ ) with (a) those using the  $\text{CIV}\lambda 1549$  emission line and the ultraviolet continuum ( $\lambda = 1350 \text{ \AA}$ ), top panel and (b) those using the  $\text{Mg II}\lambda 2798$  emission line and ultraviolet continuum at  $\lambda = 3000 \text{ \AA}$ , lower panel. The dotted line represents a 1:1 relation to aid the eye.

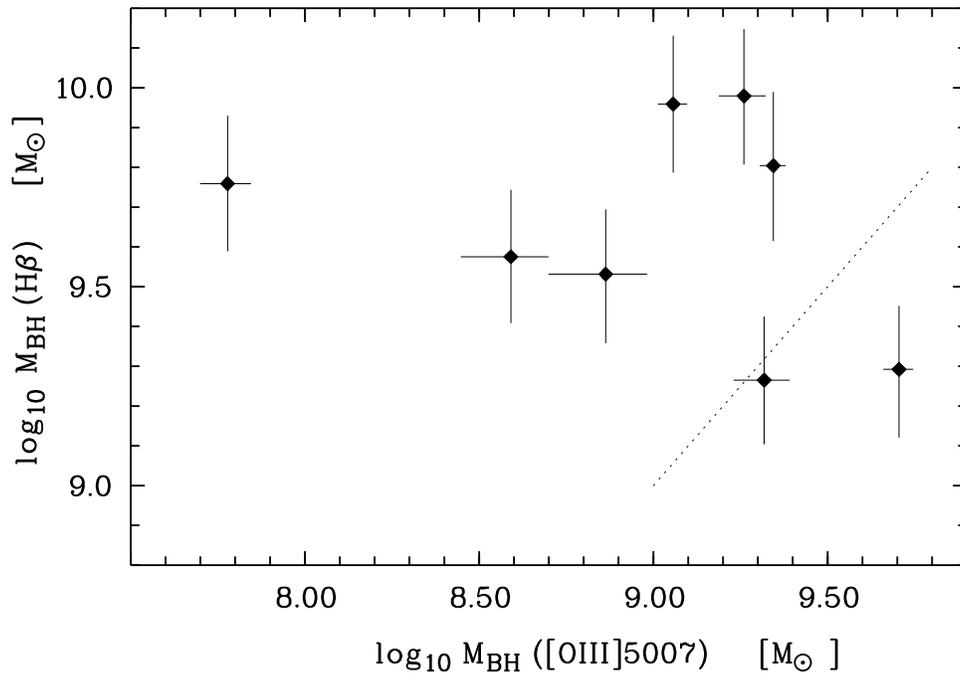


Figure 6 – The black hole mass, based on  $\text{H}\beta$ , is shown versus the mass estimated from the narrow forbidden  $[\text{O III}]\lambda 5007$  emission line profile width. The dashed line is the  $M_{bh} - \sigma_*$  (Tremaine et al. 2002). The black hole mass estimates, employing  $\text{H}\beta$ , are almost always bigger than the expected mass following the  $M_{bh} - \sigma_*$  relation.

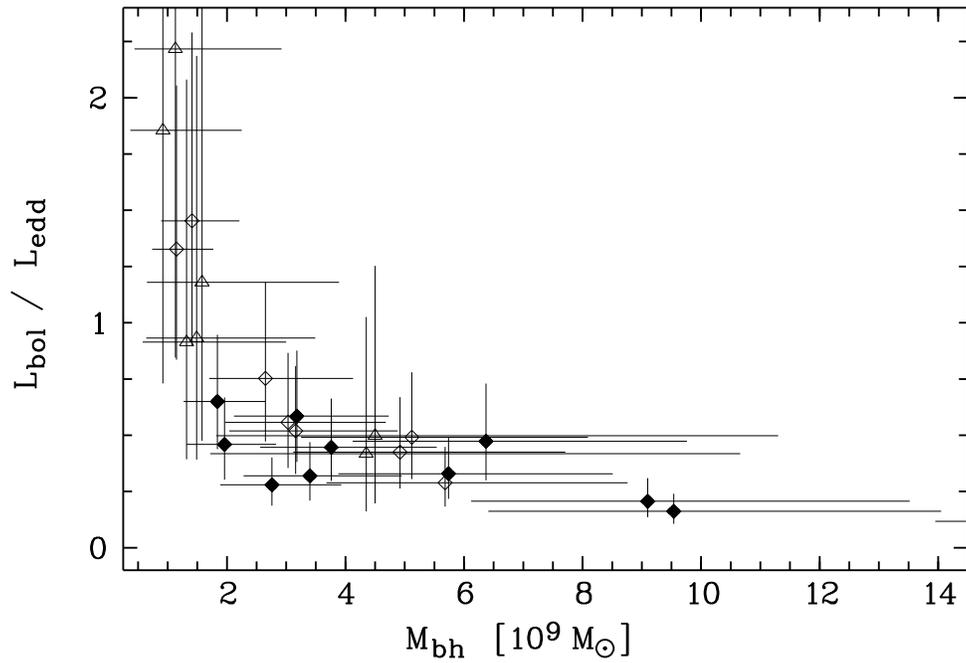


Figure 7 – The Eddington ratio  $L_{bol}/L_{edd}$ , derived for the intermediate-redshift quasars of this study, is displayed as a function of the estimated black hole masses which are based on the FWHM(H $\beta$ ) (filled diamonds), FWHM(Mg II  $\lambda$ 2798) (open triangles), and FWHM(C IV  $\lambda$ 1549) (open squares).

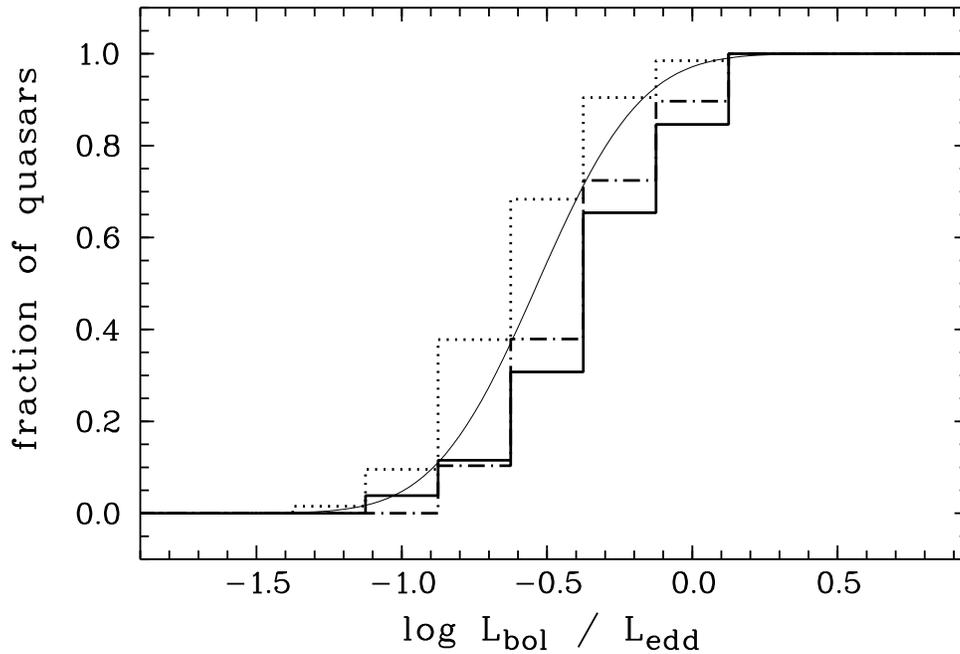


Figure 8 – The cumulative distribution of the Eddington ratio  $\log(L_{bol}/L_{edd})$  which we derive for the intermediate redshift quasars of this study, is displayed as a thick solid line.

For comparison the results of Kollmeier et al. (2006) for quasars with  $z > 1.2$  and  $L_{bol} > 10^{46} \text{ erg s}^{-1}$  is shown as dotted line together with the Gaussian model fit to their Eddington ratio distribution (thin solid line). The distribution of  $\log(L_{bol}/L_{edd})$  which has been determined by Shemmer et al. (2004) for their intermediate redshift quasars is presented as a dashed-dotted line.

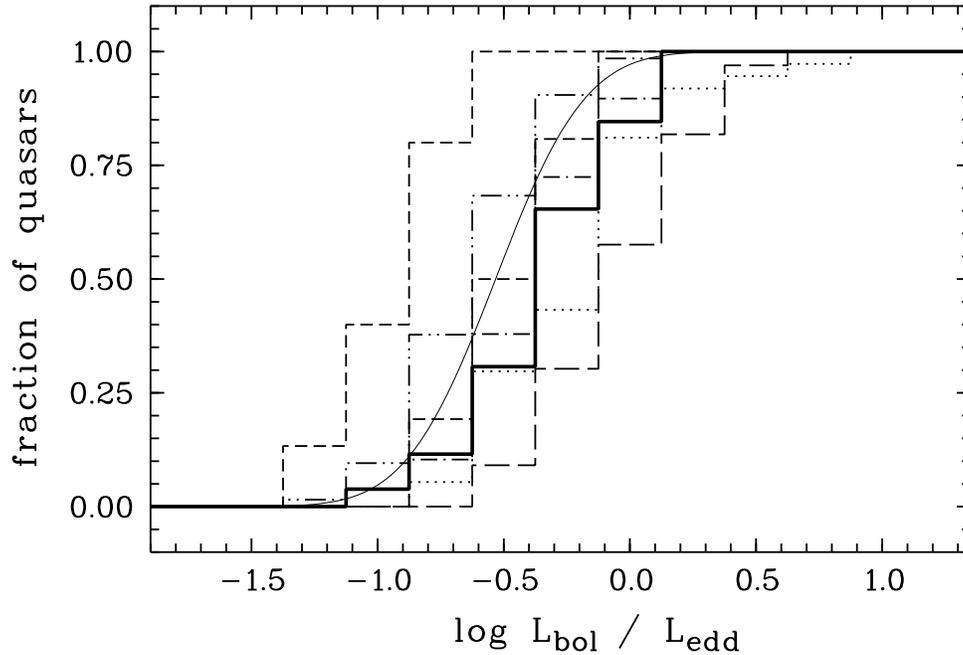


Figure 9 – The cumulative distribution of the Eddington ratios of this study (thick solid line) is compared with those of former investigation by Dietrich & Hamann (2004; long-dashed line), Kollmeier et al. (2006; dashed-dotted-dotted line), Netzer et al. (2007; short-dashed line), Shemmer et al. (2004; dashed-dotted line), Sulentic et al. (2004, 2006; short-dashed line, close to the Gaussian model fit), Yuan & Wills (2003; dotted line). In addition, the Gaussian model fit (Kollmeier et al. 2006) is displayed as a thin black line for comparison.

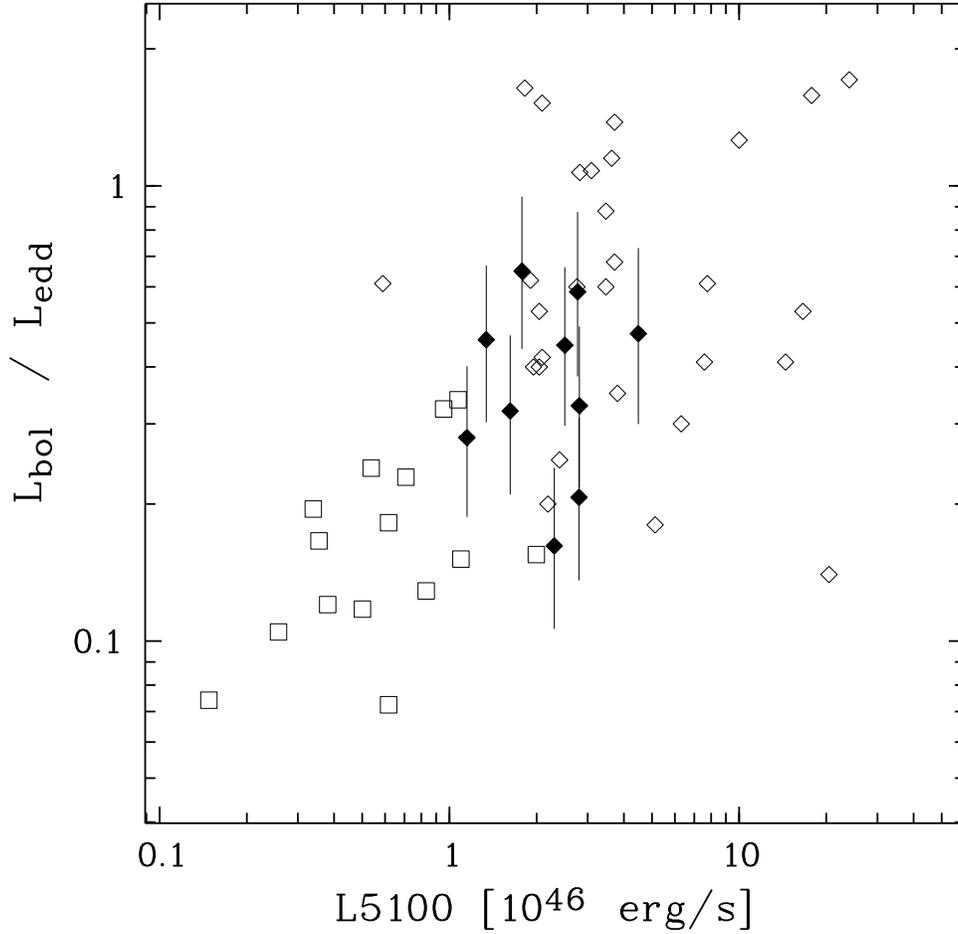


Figure 10 – The Eddington ratio  $L_{bol}/L_{edd}$  is plotted as a function of the optical continuum flux  $L(5100) = \lambda L_{\lambda}(5100\text{\AA})$  for the quasars of our study (filled diamonds). For comparison the results are displayed for the quasars of comparable luminosity presented by Shemmer et al. (2004; open diamonds) and the quasars of lower luminosity (open squares) of the Netzer et al. (2007) study.

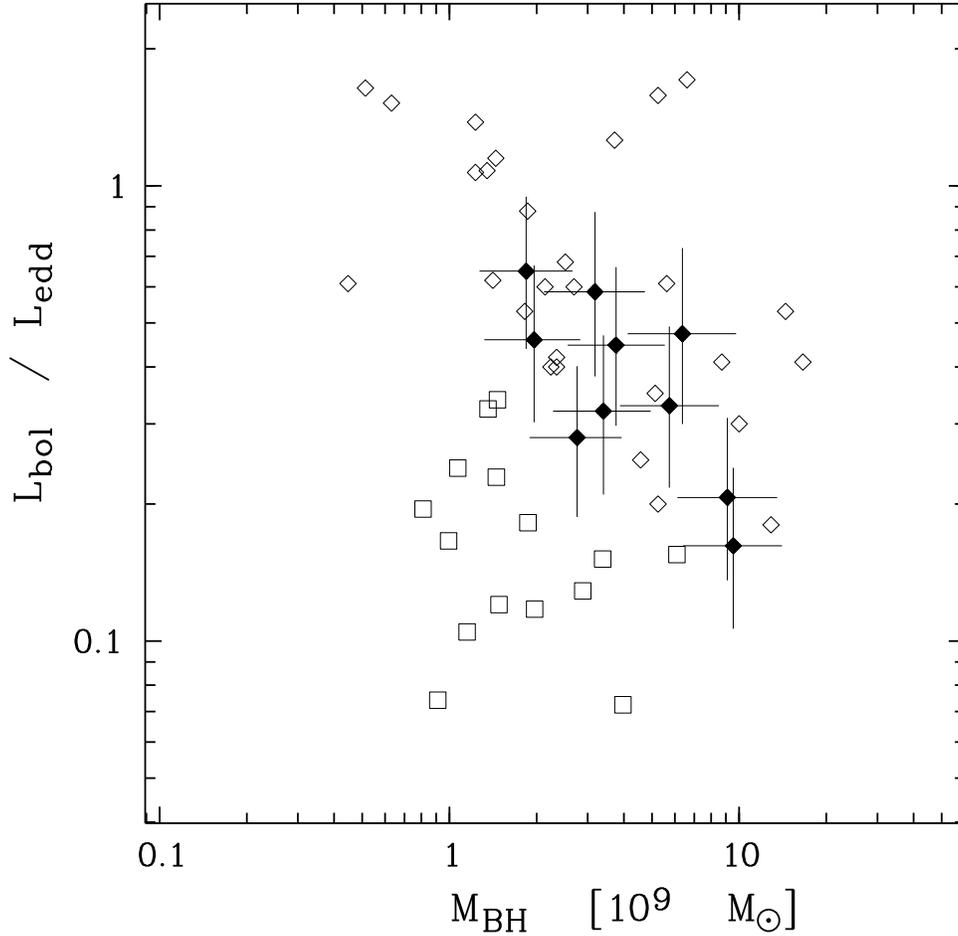


Figure 11 – The Eddington ratio  $L_{\text{bol}}/L_{\text{edd}}$  is plotted as a function of the black hole mass for the quasars of our study (filled diamonds). For comparison the results are displayed for the quasars of comparable luminosity presented by Shemmer et al. (2004; open diamonds) and the quasars of lower luminosity (open squares) of the Netzer et al. (2007) study.

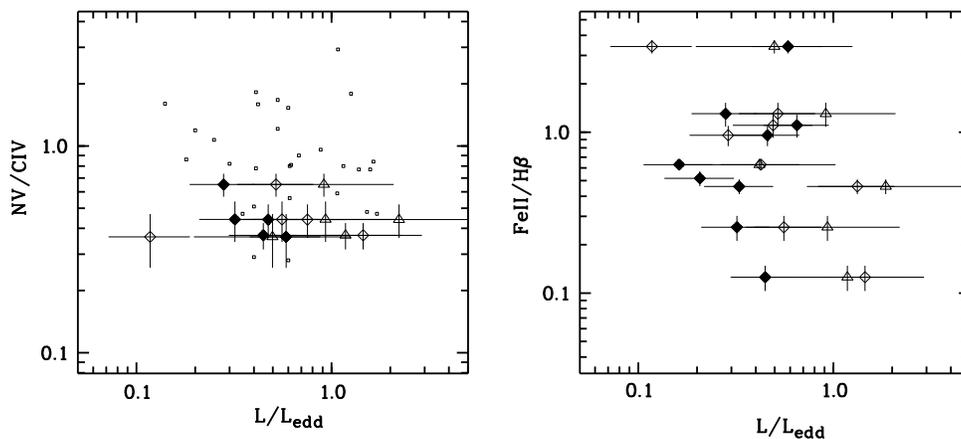


Figure 12 – The emission line ratio  $NV\lambda1240/CIV\lambda1549$  (left panel), as well as the relative strength of the optical  $FeII$ -emission,  $FeII/H\beta$  (right panel) are displayed as a function of the Eddington ratio  $L/L_{edd}$  (filled diamonds represent  $H\beta$ -based black hole mass estimates, open triangles  $MgII\lambda2798$ -based, and open diamonds  $CIV\lambda1549$ -based). For comparison the results of Shemmer et al. (2004) are shown (small open boxes).

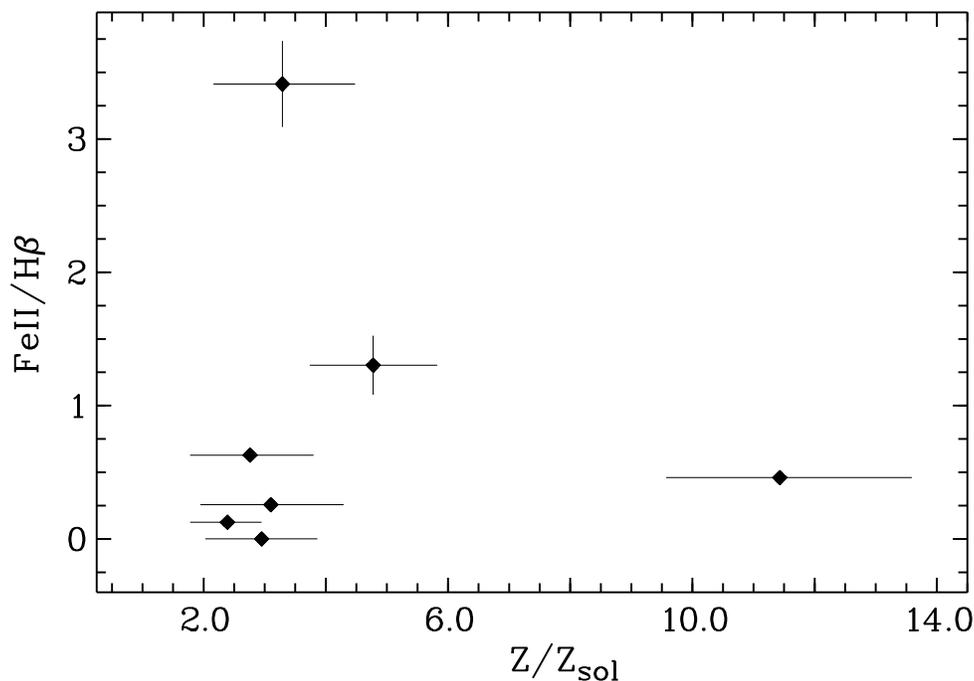


Figure 13 – The relative strength of the optical  $FeII$ -emission  $FeII/H\beta$  is plotted as a function of metallicity. Based on these measurements no clear correlation is visible between these two observables.



Table 1. Observing log of the luminous intermediate-redshift Quasars.

object (1)	RA <sup>a</sup>	DEC <sup>a</sup>	m <sub>V</sub> <sup>c</sup>	m <sub>J</sub> <sup>b</sup>	z <sup>c</sup>	B.I. <sup>d</sup>	T <sub>exp</sub> <sup>e</sup>	N <sub>exp</sub> <sup>f</sup>	AM(z) <sup>g</sup>	civil date (10)
Q 0019+0107	00 22 27.5	+01 24 12.7	18.9	16.4	2.131	2305	114	38	1.25	11-Sep-04
Q 0020–0154	00 23 02.4	–01 38 16.0	18.3	...	1.465	1502	90	30	1.77	10-Sep-04
Q 0150–202	01 52 27.3	–20 01 07.0	17.4	15.8	2.147	0	108	36	1.03	09-Sep-04
Q 0302–2223	03 04 49.9	–22 11 52.2	16.0	15.5	1.406	0	60	20	1.02	11-Sep-04
Q 2116–4439	21 20 11.5	–44 26 53.8	17.7	16.3	1.504	2594	96	32	1.09	09-Sep-04
Q 2154–2005	21 57 05.9	–19 51 13.8	18.3	16.5	2.042	962	120	40	1.15	10-Sep-04
Q 2209–1842	22 12 10.4	–18 27 37.8	17.8	16.2	2.098	0	120	40	1.23	11-Sep-04
Q 2212–1759	22 15 31.7	–17 44 08.0	18.3	16.3	2.230	2221	60	20	1.03	09-Sep-04
Q 2230+0232	22 32 35.3	+02 47 55.1	18.0	16.9	2.215	0	120	40	1.35	10-Sep-04
Q 2302+0255	23 04 45.0	+03 11 46.1	15.8	14.7	1.062	0	84	28	1.22	09-Sep-04

<sup>a</sup>right ascension and declination for J2000.0

<sup>b</sup>2 MASS magnitudes

<sup>c</sup>based on the H $\beta$ 4861 and [O III] 5007 emission lines.

<sup>d</sup>BALnicity index in units of km s<sup>–1</sup> (Bechtold et al. 2002; Hewett & Foltz 2003; Korista et al. 1993; Weymann et al. 1991)

<sup>e</sup>total integration time in minutes

<sup>f</sup>number of individual exposures

<sup>g</sup>average air mass during the observation

Table 2. Results of the H $\beta$ , [O III] $\lambda$ 5007, H $\alpha$ , Mg II $\lambda$ 2798, and C IV $\lambda$ 1549 emission line profile analysis.

object (1)	FWHM <sup>a</sup>				
	H $\beta$ 4861 (2)	[O III] $\lambda$ 5007 (3)	H $\alpha$ 6563 (4)	Mg II $\lambda$ 2798 (5)	C IV $\lambda$ 1549 (6)
Q 0019+0107	8800 $\pm$ 820	900 $\pm$ 120	...	6000 $\pm$ 940	5880 $\pm$ 480
Q 0020–0154	4120 $\pm$ 210	930 $\pm$ 150	3150 $\pm$ 290	...	5720 $\pm$ 210
Q 0150–202	6080 $\pm$ 570	940 $\pm$ 30	...	2720 $\pm$ 270	4360 $\pm$ 230
Q 0302–2223	8180 $\pm$ 490	800 $\pm$ 40	6560 $\pm$ 490	...	...
Q 2116–4439	4560 $\pm$ 660	1160 $\pm$ 70	3180 $\pm$ 600	...	6740 $\pm$ 410
Q 2154–2005	5630 $\pm$ 730	...	...	3880 $\pm$ 380	5020 $\pm$ 350
Q 2209–1842	5410 $\pm$ 180	620 $\pm$ 170	...	3570 $\pm$ 270	3170 $\pm$ 290
Q 2212–1759	6490 $\pm$ 180	380 $\pm$ 30	...	2770 $\pm$ 330	3090 $\pm$ 290
Q 2230+0232	5730 $\pm$ 780	720 $\pm$ 220	...	3850 $\pm$ 170	4890 $\pm$ 220
Q 2302+0255	4850 $\pm$ 410	...	3490 $\pm$ 90	5730 $\pm$ 310	11800 $\pm$ 1020

<sup>a</sup>The full-width-at-half-maximum (FWHM) is given in units of km s<sup>–1</sup> (corrected for spectral resolution, R = 540 km s<sup>–1</sup>).

Table 3. Emission Line Ratios and Gas Metallicity Estimates

object (1)	line ratio				$Z/Z_{\odot}$			
	N v/ C iv (2)	N v/ He II (3)	N iv]/ C iv (4)	N iii]/O iii] (5)	N v/ C iv (6)	N v/ He II (7)	N iv]/ C iv (8)	N iii]/O iii] (9)
Q 0019+0107	...	$13.90 \pm 3.79$	...	$0.77 \pm 0.30$	...	$> 10$	...	$2.8^{+9.0}_{-1.0}$
Q 0020–0154	...	...	...	...	...	...	...	...
Q 0150–202	$0.44 \pm 0.08$	$6.29 \pm 1.55$	$0.15 \pm 0.02$	$0.45 \pm 0.09$	$4.1^{+0.9}_{-0.9}$	$17.8^{+6.3}_{-7.0}$	$4.7^{+0.6}_{-0.7}$	$1.8^{+0.2}_{-0.3}$
Q 0302–2223	...	...	...	...	...	...	...	...
Q 2116–4439	...	...	...	...	...	...	...	...
Q 2154–2005	$0.60 \pm 0.07$	$3.53 \pm 0.55$	...	$0.86 \pm 0.17$	$5.9^{+0.8}_{-0.7}$	$6.2^{+1.9}_{-1.6}$	...	$3.1^{+0.6}_{-0.6}$
Q 2209–1842	$0.37 \pm 0.05$	$2.85 \pm 0.48$	$0.02 \pm 0.01$	$0.32 \pm 0.07$	$3.4^{+0.5}_{-0.6}$	$4.5^{+1.2}_{-0.8}$	$0.6^{+0.3}_{-0.3}$	$1.4^{+0.2}_{-0.2}$
Q 2212–1759	...	...	...	$2.93 \pm 0.42$	...	...	...	$11.4^{+1.9}_{-1.6}$
Q 2230+0232	$0.44 \pm 0.10$	$4.42 \pm 1.25$	...	$0.56 \pm 0.15$	$4.2^{+1.0}_{-1.1}$	$9.6^{+5.5}_{-4.5}$	...	$2.0^{+0.5}_{-0.4}$
Q 2302+0255	$0.30 \pm 0.08$	...	...	...	$2.7^{+0.8}_{-0.8}$	...	...	...

Table 4. Black hole mass estimates following Vestergaard & Peterson (2006) for H $\beta$  and C iv $\lambda$ 1549 and McLure & Dunlop (2004) for Mg II $\lambda$ 2798.

object (1)	$L(5100)$ (2)	$L(3000)$ [ $10^{46}$ erg s $^{-1}$ ] (3)	$L(1350)$ (4)	H $\beta$ 4861 (5)	$M_{BH}$ [ $10^9 M_{\odot}$ ] <sup>b</sup>		
					Mg II $\lambda$ 2798 (6)	Mg II $\lambda$ 2798 <sup>a</sup> (7)	C iv $\lambda$ 1549 (8)
Q 0019+0107	2.30	3.49	6.56	$9.5^{+4.5}_{-3.1}$	$4.4^{+6.3}_{-2.6}$	$13.5^{+6.4}_{-4.4}$	$4.9^{+2.8}_{-1.8}$
Q 0020–0154	1.78	...	7.89	$1.8^{+0.8}_{-0.6}$	...	...	$5.1^{+3.0}_{-1.9}$
Q 0150–202	4.49	5.13	9.33	$6.4^{+3.4}_{-2.2}$	$1.1^{+1.8}_{-0.7}$	$3.4^{+1.8}_{-1.2}$	$3.3^{+2.0}_{-1.2}$
Q 0302–2223	2.80	...	...	$9.1^{+4.4}_{-3.0}$	...	...	...
Q 2116–4439	1.34	...	5.15	$2.0^{+0.9}_{-0.6}$	...	...	$5.7^{+3.1}_{-2.0}$
Q 2154–2005	1.82	2.68	4.80	$4.4^{+2.0}_{-1.5}$	$1.4^{+1.9}_{-0.8}$	$4.3^{+1.8}_{-1.4}$	$3.2^{+1.7}_{-1.1}$
Q 2209–1842	2.50	3.65	6.43	$3.2^{+1.5}_{-1.0}$	$1.6^{+2.3}_{-0.9}$	$4.9^{+2.3}_{-1.6}$	$1.4^{+0.8}_{-0.5}$
Q 2212–1759	2.81	3.48	4.79	$5.2^{+2.5}_{-1.7}$	$0.9^{+1.3}_{-0.5}$	$2.9^{+1.4}_{-0.9}$	$1.2^{+0.6}_{-0.4}$
Q 2230+0232	1.62	2.60	5.30	$3.4^{+1.5}_{-1.1}$	$1.5^{+2.0}_{-0.8}$	$4.8^{+2.2}_{-1.6}$	$3.0^{+1.6}_{-1.1}$
Q 2302+0255	2.77	4.27	8.23	$3.2^{+1.6}_{-1.1}$	$4.5^{+6.8}_{-2.7}$	$13.6^{+6.6}_{-4.5}$	$22.3^{+13.1}_{-8.4}$

<sup>a</sup>assuming a fixed slope of  $\beta = 0.5$  for the R–L relation and  $D = (2.0 \pm 0.5) 10^8 M_{\odot}$  (see § 5.1)

<sup>b</sup>based on the emission line profile widths as given in Table 2 and the continuum luminosity ( $L = \lambda L_{\lambda}$ ) measured at  $\lambda = 5100 \text{ \AA}$  (2),  $\lambda = 3000 \text{ \AA}$  (3), and  $\lambda = 1350 \text{ \AA}$  (4), respectively.

Table 5. Bolometric luminosities and Eddington ratios

object	$L_{bol}$ [ $10^{47}$ erg $s^{-1}$ ]			$L_{edd}^{a,b}$ [ $10^{47}$ erg $s^{-1}$ ]			$H\beta$	$L_{bol}/L_{edd}$	
	$\lambda 5100$	$\lambda 1350$	mean( $L_{bol}$ )	$H\beta$	Mg II $\lambda 2798$	C IV $\lambda 1549$		Mg II $\lambda 2798^c$	C IV $\lambda 1549$
(1)	(2)	(3)	(4)	(5)	(6)	(7)	(8)	(9)	
Q 0019+0107	2.24	3.03	2.64	13.83	6.31	7.13	0.16	0.42	0.43
Q 0020–0154	1.73	3.65	2.69	2.67	...	7.42	0.65	...	0.49
Q 0150–202	4.37	4.31	4.34	9.24	1.64	4.73	0.47	2.22	0.75
Q 0302–2223	2.73	...	2.73	13.20	...	...	0.21	...	...
Q 2116–4439	1.31	2.38	1.84	2.84	...	8.24	0.46	...	0.29
Q 2154–2005	1.77	2.22	2.00	6.32	2.00	4.68	0.28	0.91	0.52
Q 2209–1842	2.44	2.97	2.70	4.67	2.29	2.05	0.45	1.18	1.45
Q 2212–1759	2.74	2.21	2.48	7.53	1.33	1.67	0.33	1.86	1.33
Q 2230+0232	1.58	2.45	2.01	4.93	2.16	4.39	0.32	0.93	0.56
Q 2302+0255	2.70	3.80	3.25	4.66	6.53	32.35	0.59	0.50	0.12

<sup>a</sup>  $L_{edd} = 1.45 \cdot 10^{38} M_{bh}/M_{\odot}$ ,  $\mu = 1.15$  (mixture of H and He gas)

<sup>b</sup> based on the corresponding black mass estimates (Table 4)

<sup>c</sup> assuming mean- $L_{bol}$

Table 6. Black hole growth time estimates (in units of Gyr), using black hole masses based on  $H\beta$  profile properties and the continuum luminosity  $L(5100)$

object	$L_{bol}/L_{edd} = 1.0$			$L_{bol}/L_{edd}$ obs. <sup>a</sup>			age of the universe [ $10^9$ yr]
	$M_{bh}(\text{seed})$			$M_{bh}(\text{seed})$			
(1)	$10 M_{\odot}$	$10^3 M_{\odot}$	$10^5 M_{\odot}$	$10 M_{\odot}$	$10^3 M_{\odot}$	$10^5 M_{\odot}$	(8)
Q 0019+0107	0.90	0.70	0.50	5.63	4.38	3.13	2.95
Q 0020–0154	0.83	0.63	0.43	1.28	0.97	0.66	4.17
Q 0150–202	0.88	0.68	0.48	1.87	1.45	1.02	2.93
Q 0302–2223	0.90	0.70	0.50	4.29	3.33	2.28	4.31
Q 2116–4439	0.83	0.63	0.43	1.80	1.37	0.93	4.08
Q 2154–2005	0.87	0.67	0.47	3.11	2.39	1.68	3.07
Q 2209–1842	0.85	0.65	0.45	1.89	1.44	1.00	3.00
Q 2212–1759	0.87	0.67	0.47	2.64	2.03	1.42	2.23
Q 2230+0232	0.86	0.66	0.45	2.69	2.06	1.41	2.92
Q 2302+0255	0.85	0.65	0.45	1.44	1.10	0.76	5.36

<sup>a</sup>  $L_{bol}/L_{edd}$  are based on the Eddington ratio estimates using  $H\beta$  (Table 5)